X.2

Area change during kink band evolution; examples from the Late Variscan of Portugal

Index

X.2.1. Introduction

Kink bands are a common subject in engineering, earth sciences and physics (Anderson, 1964; Jensen, 1999; Qiao and Winey, 2000; Wadee et al., 2003; Wadee and Edmunds, 2005). They are associated with deformation in solids usually with a strong planar mechanical anisotropy and could occurred at all scales (Anderson 1964; Matte, 1969; Jensen, 1999; Wadee and Edmunds, 2005).

In earth sciences, the kink bands are common in rocks with a strong planar anisotropy (*e.g.* bedding, slaty cleavage or foliation), like shales, slates, phyllites or schists (Anderson 1964; 1974; Dewey, 1965; Matte, 1969; Williams, 1987; Twiss and Moores, 1992) and are found from mineralogical (Starkey, 1968; Tchalenko, 1968; Misra and Burg, 2012; Goswami, 2013) to orogenic scales (Collomb and Donzeau, 1974; Goscombe et al., 1994; Suppe et al., 1997; Pachell et al., 2003). Although anisotropy favours the development of kink bands, occasionally they are also found in isotropic rocks (Borg and Handin, 1966; Hanmer, 1982;

Davies and Pollard, 1986; Williams, 1987; Pachell et al., 2003). The understanding of the genetical processes related to such diversity give rise to several approaches: experimental works (Paterson and Weiss, 1962; Borg and Handin, 1966; Paterson and Weiss, 1966; Donath, 1968; Cobbold *et al.*, 1971; Anderson, 1974; Gay and Weiss, 1974; Stewart and Alvarez, 1991; Hanmer et al., 1996 Wadee *et al.*, 2003), field based studies (Anderson, 1964; Matte, 1969; Babaie and Speed, 1990; Stubley, 1990; Sharma and Bhola, 2005) as well as theoretical studies (Dewey, 1969; Weiss, 1980; Srivastava et al., 1998).

Previous studies led to two main models for the origin of kink bands (*e.g.* Stewart and Alvarez, 1991; Twiss and Moores, 1992): the mobile-hinge and the fixed-hinge models. The first emphasize the gradual growth of kink bands, either by lateral or rotational migration of their boundaries. In the fixed-hinge model, the boundaries are fixed, being the rotation restricted to the internal domain. Although both models enhanced some of the processes related to the genetic mechanisms and geodynamic significance of these structures, the fixed-hinge models did not explain/discuss the inevitable area change within the kink band. Detailed geometrical and kinematical analysis of two mesoscopic late Variscan kink bands in Iberia help, not only to understand the internal distortion related to fixed hinged kink bands, but also to establish a new graphical method to quantify this distortion.

X.2.2. Kink Band structures overview

Kink bands are common in polydeformed areas, being generally generated under low-grade metamorphic conditions; they usually occur in brittle or brittle-ductile regime during late tectonic events (Anderson, 1964; Dewey, 1965; Suppe 1985; Babaie and Speed, 1990; Sharma and Bhola, 2005). These structures mostly result from layer parallel shortening in anisotropic rock induced by a major compression nearly parallel to previous layering (e.g. Anderson 1964; 1974; Hanmer et al., 1996).

The diversity of studies and models concerning kink-bands, led to a strong disparity of the parameters that have been used, turning useful a summary overview of previous works.

X.2.2.1. Kink Band Geometrical and Kinematical features

Kink bands are asymmetric folds with straight limbs and sharp hinges (fig. 1; Ramsay and Huber, 1987; Stewart and Alvarez, 1991; Twiss and Moores, 1992). Kink folds have a short limb (kink band) restrained between two axial surfaces (kink band boundaries) and two undeformed long limbs (Anderson 1964; 1974; Dewey, 1965; Weiss, 1980; Stewart and Alvarez, 1991; Twiss and Moores, 1992). These structures are usually characterized using three angular parameters (fig. 1):

- ϕ is the angle between the planar anisotropy outside the kink band and the kink plane (Paterson and Weiss, 1966; Weiss, 1980; Srivastava et al., 1998; also called α by Anderson, 1964; 1974; Dewey, 1965; Ramsay and Huber, 1987);

- ϕk express the angular parameter between the kink plane and the planar anisotropy inside the kink band (Paterson and Weiss, 1966; Weiss, 1980; Srivastava et al., 1998; also called β by Anderson, 1964; 1974; Dewey, 1965; Ramsay and Huber, 1987);

- ψ is considered the kink angle (Twiss and Moores, 1992) and gives the angular relation between the planar anisotropy outside and inside the kink band.

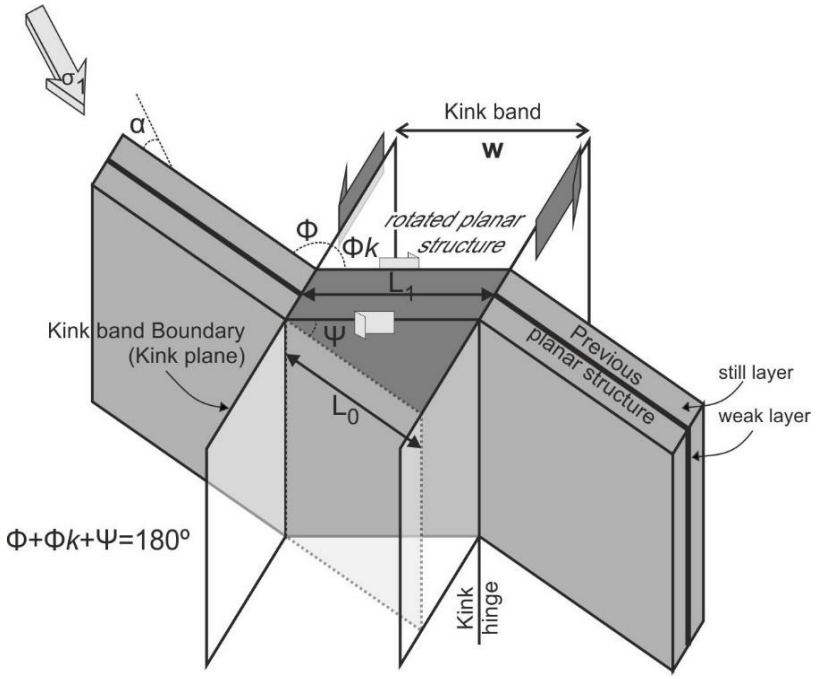

Figure 1 – Geometric and kinematic features of kink bands (adapted from Gay and Weiss, 1974; Srivastava et al., 1998).

Previous angular parameters are not independent (Weiss, 1980; Srivastava et al., 1998):

$$\phi + \phi k + \psi = 180º \text{ (equation 1)}$$

Natural and experimental studies show that kink bands can appeared, either as individual monoclinal sets or two conjugate sets with opposite kinematics (Dewey, 1969; Paterson and Weiss, 1966; Anderson, 1974; Suppe, 1985; Babaie and Speed, 1990).

X.2.2.2. Stress and Strain in Kink Bands

Experimental works on rock mechanics of foliated rocks (Paterson and Weiss, 1962; 1966; Borg and Handin, 1966; Donath, 1968; Gay and Weiss, 1974) and analogical modelling

(Cobbold et al., 1971; Gay and Weiss, 1974; Williams and Price, 1990; Stewart and Alvarez, 1991) show that in kink bands the major principal stress ($\sigma 1$) is parallel or close to the direction of main foliation (Donath, 1961; Anderson, 1964; 1974; Paterson and Weiss, 1962; Gay and Weiss 1974; Williams and Price, 1990). When conjugate kink bands are developed, their geometry and kinematics can be used to determine the three dimensional stress field orientation (Ramsay, 1962; Gay and Weiss, 1974; Tobisch and Fiske, 1976; Suppe, 1985), using the bisectors of the dihedral angles between the conjugate pairs of kink planes (Ramsay, 1962; Tobisch and Fiske, 1976; Stewart and Alvarez, 1991).

Previous relations are valid for pure shear kink bands, but kink-bands could also be developed in a simple shear regime (Stubley, 1990; Williams and Price, 1990). In this case, the 'conjugate bisector' method should be used with caution, because stress could have been variable during folding, modifying in ± 20º the orientation of maximum and minimum strain axis (Ramsay 1967; Stubley, 1990; Williams and Price, 1990).

The formation of one or the two conjugate sets of kink folds depends of the obliquity between the shortening and the main layering (fig. 2; Paterson and Weiss, 1962; 1966; Cobbold et al., 1971; Gay and Weiss, 1974; Williams and Price, 1990; Stubley, 1990). For very low obliquities ($\alpha \leq 5º$; fig. 1) experimental data shows that symmetric conjugate kink bands are developed (fig. 2; Paterson and Weiss, 1962; 1966; Donath, 1968; Cobbold et al., 1971; Anderson, 1974; Gay and Weiss, 1974; Stewart and Alvarez, 1991). With α increase, one set of kink bands starts to prevail and the asymmetry becomes evident. When α attain more than 10º, generally only one set is generated (Paterson and Weiss, 1962; 1966; Cobbold et al., 1971; Gay and Weiss, 1974). However for higher obliquities ($\alpha \geq 30º$) development of kink bands seems to be negligible (Paterson and Weiss, 1966; Donath, 1968; Gay and Weiss, 1974), and sliding along the foliation prevails (fig. 2).

X.2.2.3. Kink Bands Genetic Models

The work done by several authors (Paterson and Weiss, 1966; Anderson, 1974; Gay and Weiss, 1974; Verbeek, 1978; Weiss, 1980; Stewart and Alvarez, 1991) allows to distinguish two main models for kink band development (mobile-hinge and fixed-hinge models), with distinct characteristics summarized in figure 3 and table I.

Mobile-hinge models

In this model kink bands initiates as a small lenticular structure and grow laterally by hinge migration, incorporating more undeformed material (Paterson and Weiss, 1966; Gay and

Weiss, 1974; Weiss, 1980; Stubley, 1990; Stewart and Alvarez, 1991). The growth of the kink bands, with the migration of the hinges could be done either by rotation (type I; fig. 3A) or by lateral migration of kink band boundaries (type II; fig. 3B; table I). Whatever the situation, both types dominates when the confining pressure is high (Gay and Weiss, 1974; Weiss, 1980; Stewart and Alvarez, 1991).

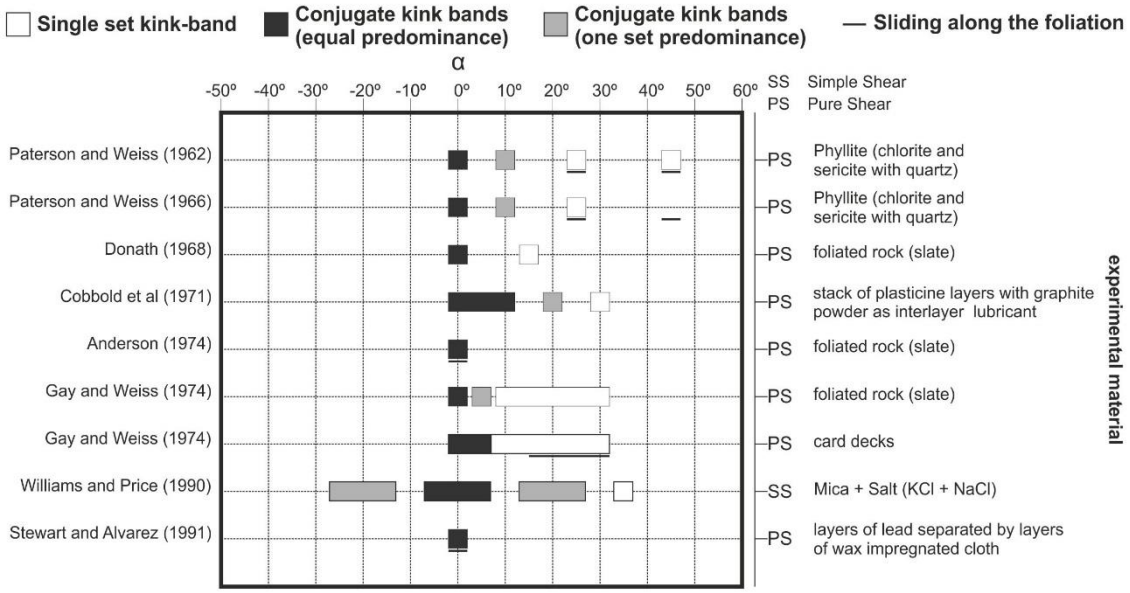

Figure 2 – Experimental relation between the geometry and kinematic of kink bands and the related stress field orientation (α angle).

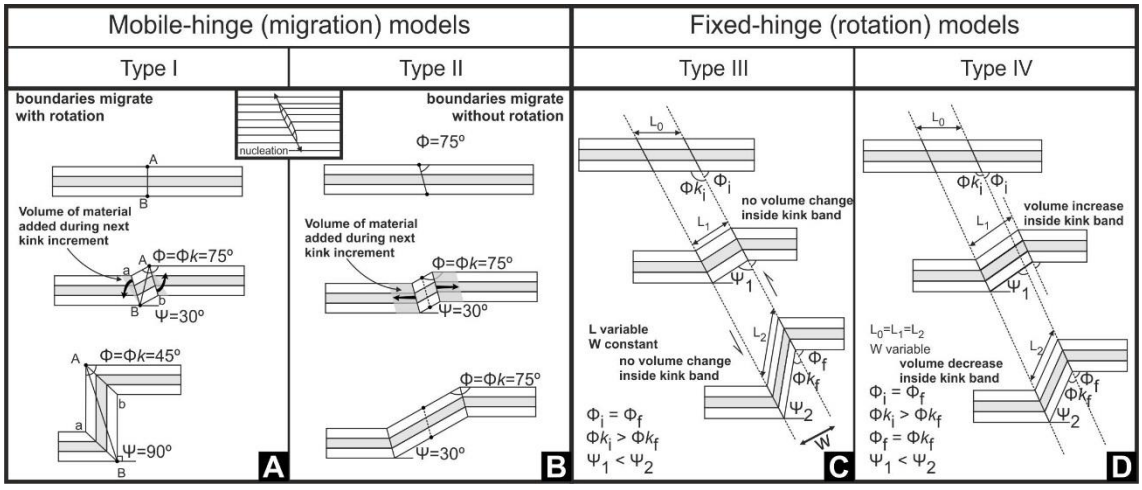

Figure 3 – Main models inducing kink band development (adapted from Twiss and Moores, 1992):

A – Mobile-hinge by boundaries migration with rotation;

B – Mobile-hinge with boundaries migration by lateral propagation

C - Fixed-hinge with simple shear kinking;

D - Fixed-hinge with rigid rotation of internal foliation.

Table I – Main geometric and kinematic characteristics of four types of kink band.

	Mobile-hinge models		**Fixed-hinge models**	
	Type I	Type II	Type III	Type IV
Deformation mechanism	Rotation and migration of hinges	Lateral migration of hinges, without rotation	Simple shear along kink band boundaries	Rigid rotation of internal foliation
ϕk and ϕ	Both decrease progressively but always $\phi k=\phi$	$\phi k=\phi$=constant is satisfied during all process	$\phi k \neq \phi$; ϕ remains constant but ϕk decreases progressively	ϕ remains constant but ϕk decreases progressively until $\phi k=\phi$
ψ	Increases progressively until 90º	Remains constant	Increases progressively	Increases progressively until locking when $\phi k=\phi$
Boundaries	Migrate by rotating about fixed hinges. The amount of rotation for both boundaries is equal but their sense of rotation are opposite	Migrate laterally away from each other by moving parallel to the initial orientation	Remain fixed during the growth	Remain fixed during the growth
Interlayer slip	Yes	Yes(?)	Yes	Yes
Total volume	Remains constant	Remains constant	Remains constant	First increases and then decreases
Width (W)	Increases by incorporation of new material	Increases by incorporation of new material	Remains constant	Variable
Length (L) of internal foliation	Increase during migration, but remains constant during the growth	Increase during migration, but remains constant during the growth	Variable	Remains constant during the growth

Fixed-hinge models

In this model the main layering rotates between two fixed boundaries, while the orientation of the kink plane remain unchanged (Twiss and Moores, 1992). The deformation associated with such kink band growth ceases when ϕ and ϕk angles are equal (Verbeek, 1978; Stewart and Alvarez, 1991). This general deformation pattern could be attained by two different type mechanisms (table I; Twiss and Moores, 1992): in type III (Fig. 3C), kink band produces a deformation equivalent to a homogeneous simple shear parallel to kink band boundaries, while type IV involves a flexural shear mechanism with shearing parallel to the laminations (Fig. 3D).

The relationship between ϕ and ϕk angles have been used to discriminate between mobile-hinge or fixed-hinge models (Anderson, 1974; Gay and Weiss, 1974; Verbeek, 1978; Stewart and Alvarez, 1991). In mobile-hinge kink bands these two angular parameters are equal, whereas fixed-hinge ones should generally have $\phi < \phi k$ (Stewart and Alvarez, 1991). However, small amounts of slip parallel to layering (in or outside of kink band) can produce a fairly large difference in angular values.

The projection of the kink band angular values in a triangular diagram (Srivastava et al., 1998), allows to assign a genetic model to kink bands (Fig. 4). However, in some natural cases, neither the hinge-migration nor the fixed-hinge model can solely explain the geometry of kink bands (Stubley, 1990). It is also possible to consider hybrid models, which involve rotation of the kinked limb and migration of its boundaries (Twiss and Moores, 1992).

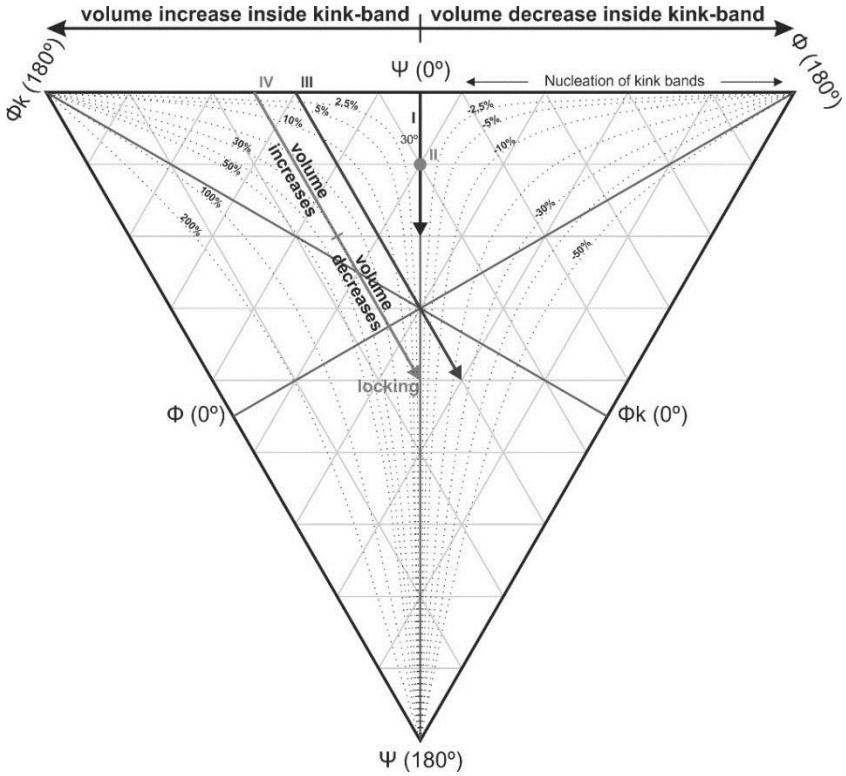

Figure 4 – Triangular diagram for kink band genetical models (adapted from Srivastava et al., 1998).

All the four types of mechanisms could involve a shear component parallel to the main layering inside the kink band, as well as preservation of continuity between planar structures across the kink band boundaries (Stewart and Alvarez, 1991; Twiss and Moores, 1992; Dunham et al., 2011). The internal interlayer slip is always anthithetical in relation to kink band kinematics (e.g. Anderson, 1964; Dewey, 1965; Matte, 1969; Verbeek, 1978; Twiss and Moores, 1992; Dunham et al., 2011). The presence of a synthetical shear component parallel to the layering in the external domains of the kink band is sometimes found (Stubley, 1990; Stewart and Alvarez, 1991).

X.2.3. Late Variscan Deformation in the Iberian Massif

The intracontinental deformation related to the late stages of the Variscan Orogeny, was induced by the dextral oblique collision between Laurentia and Gondwana (Arthaud and

Matte, 1977; Shelley and Boussiére, 2002; Nance et al., 2012; Dias et al., 2016a). Such regime is expressed in Iberia by E-W lithospheric dextral transcurrent shear zones (Fig. 5A; e.g. Ribeiro, 2002; Ribeiro et al., 2007; Denèle et al., 2014; Dias et al., 2015; 2016b), which have been strongly reworked during Meso-Cenozoic times, controlling either the Cantabro-Pyrenean chain at North or the complex the Azores-Gibraltar plate boundary at south (Ribeiro, 2002).

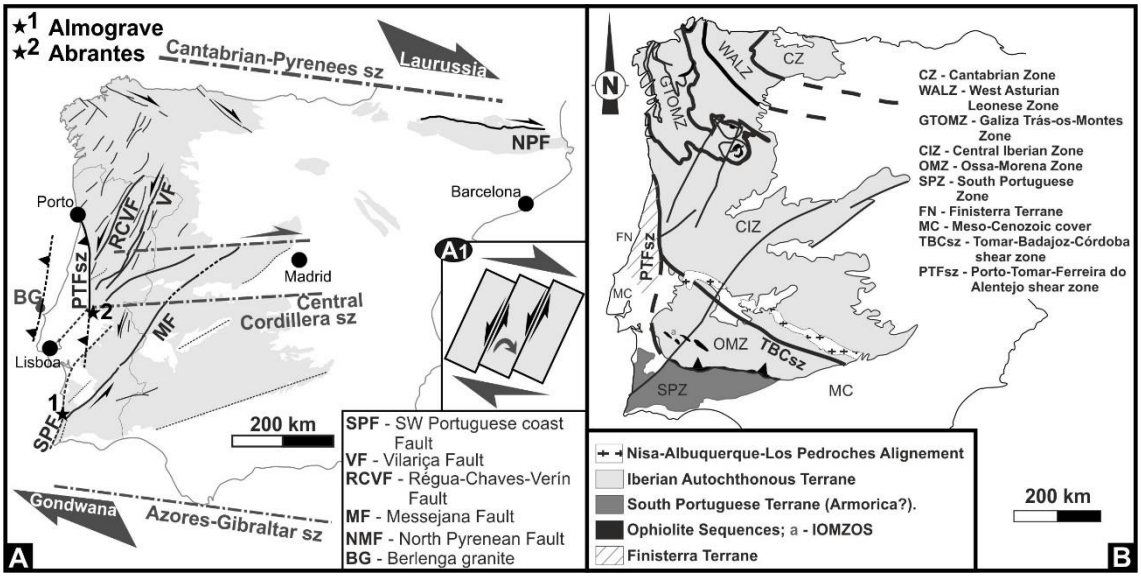

Figure 5 – General features of Iberian Variscides:

A – Late Variscan fracture pattern of Iberia, with localization of studied kink band structures, displaying the interpretative model of clockwise rotation of blocks bounded by NNE–SSW faults in a domino deformation model (a_1; adapted from Dias et al., 2016b);

B – Main Variscan tectonostratigraphic zones and Terranes of Iberia Variscides (adapted from Ribeiro et al., 2007; Romão et al., 2014; Dias et al., 2016a).

Although the main dextral plate collision is accepted, there are some debate concerning the kinematics of the NNE-SSW to NE-SW 2nd order fracture pattern in Iberia (Fig. 5A;-Dias et al., 2016b for a discussion). While most authors consider these late Variscan faults as sinistral (Arthaud and Matte, 1977; Choukhroune and Iglésias, 1980; Iglesias and Ribeiro, 1981; Pereira et al., 1993; Caroça and Dias, 2002; Moreira et al., 2010; 2014; Dias and Basile, 2013; Dias et al., 2013; 2016b), in some works a dextral Variscan kinematics is assumed being the sinistral kinematics ascribed to the Alpine reworking (Marques et al., 2002; 2010; Lourenço et al., 2002).

The dextral kinematics emphasized by Marques et al (2002) in Central Iberian Zone NNE-SSW faults was dated as late Carboniferous (ca. 312 Ma obtained in K–Ar in muscovite concentrates of fault related rocks). Although these authors considered this age a lower limit

for the Late Variscan event, it could also be consider the upper limit for the D_3 Variscan regional event (Dallmeyer et al., 1997; Dias et al., 2016b), where such trends have also a right-lateral kinematic (Pereira et al., 1993; Mateus and Noronha, 2010). The NNE-SSW sinistral kinematics have been confirmed, either by AMS studies in Vila Pouca de Aguiar and Pedras Salgadas D_3 granites (Sant'Ovaia et al., 2000; Sant'Ovaia e Noronha, 2005) of 300 Ma (Martins et al., 2009), or structural detailed data in South Portuguese Zone, where their kinematics were interpreted as the result of a domino mechanism associated with the 1st order E-W transcurrent dextral shear zones (Fig. 5A; Dias et al., 2016b).

X.2.4. Geometric and Kinematic analysis in Late Variscan Kink Bands of Portugal

In the Iberian Variscides the pervasive brittle to brittle-ductile late Variscan fracture pattern is often related to mesoscopic kink band structures. In Almograve region these structures were mostly induced by discrete NNE-SSW sinistral strike-slip faults (Caroça and Dias, 2002; Dias and Basile, 2013; Dias et al., 2016b). The same geometry and kinematics have also been described in Abrantes region (Moreira, 2012). In both cases the good outcrop conditions help to enhance the understanding of their genetic mechanisms.

X.2.4.1. Almograve Kink Bands

The Almograve region (Fig. 6) is located in the South Portuguese Zone (Fig. 5B), a Variscan foreland belt with a SW facing imbricated fold and trusts (Ribeiro et al., 2007; Marques et al., 2010). In Almograve, this complex is a low-grade metamorphic flysch sequence, composed of interlayered greywackes, quartzwackes and shales beds (Marques et al., 2010; Dias and Basile, 2013).

This sequence was deformed by two main Variscan deformation episodes (Dias and Basile, 2013; Dias et al., 2016b). While the first (D_1) is a pervasive deformation giving rise to the NNW-SSE regional structure, the second deformation (D_2) is a discrete event mostly concentrated along NNE-SSW deformation bands (Fig. 6) which is a common situation in the Iberian Variscides (e.g. Dias et al., 2013; 2016b; Moreira et al., 2014).

The D_1 episode in Almograve is the result of a coaxial progressive deformation developed in a low structural level (Marques et al., 2010; Dias and Basile, 2013; Dias et al., 2016b), whose pervasive deformation helps to constrain the D2 geometry and kinematics. The most obvious D_1 structures are general NNW-SSE (N30ºW to N20ºW) orthorhombic upright folds with subvertical axial planes and subhorizontal hinges (less than 10º; Figs. 6 and 7A). Mostly in the hinge zones and in the more fine-grained lithotypes an axial planar S_1 cleavage is found (Fig. 7B), which gives rise to an intersection lineation L_1 (S_0^S_1) parallel to the fold hinges.

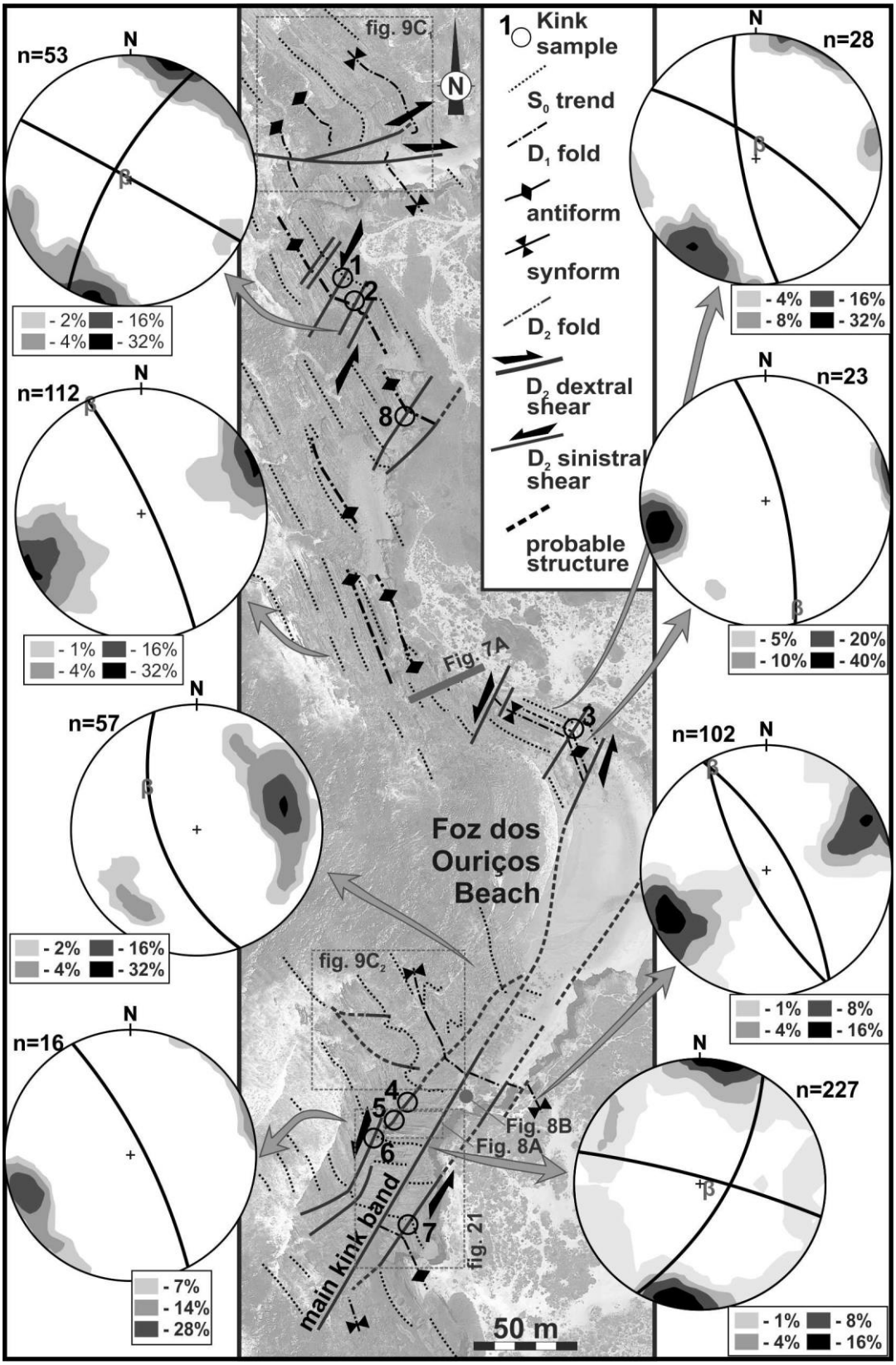

Figure 6 –Structural map of Almograve Kink band emphasizing the heterogeneous geometrical behaviour of bedding due to the interference between both Variscan deformation events (equal area lower hemisphere stereographic projections of S_0).

The late stages of D_1 give rise to sub-vertical brittle to brittle-ductile conjugate shear zones (with an acute angle between them of 60º: Fig, 7C) better expressed in the strongly dipping limbs of D_1 early folds: N-S to NNE-SSW dextral and sinistral ENE-WSW to E-W. This shows a stress field with a NE-SW σ_1 and a NW-SE σ_3 both sub-horizontal and a sub-vertical σ_2. Such stress field is compatible with D_1 folds that are thus considered developed in the same tectonic event (Dias and Basile, 2013; Dias et al., 2016b).

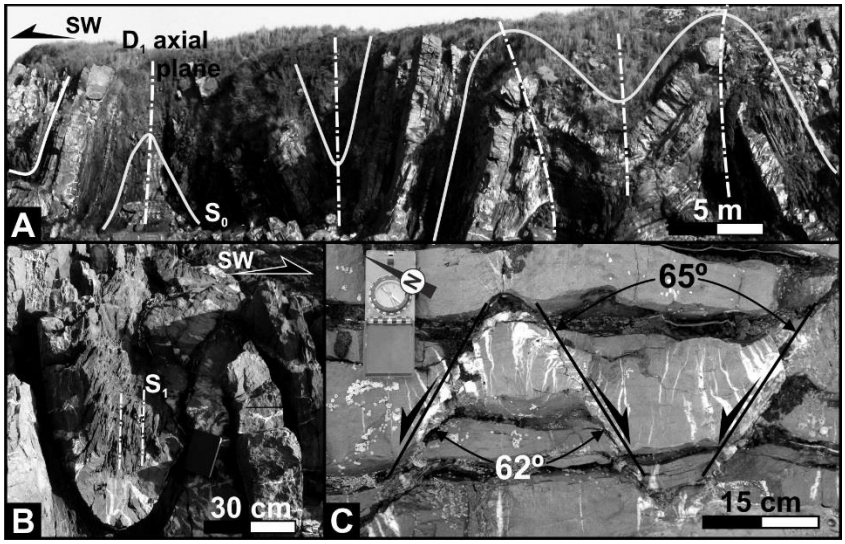

Figure 7 – Geometrical and kinematical features of D_1 structures:

A –D_1 folds general pattern;

B – Axial planar S_1 cleavage in D_1 tight folding;

C – Late D_1 conjugate shear zones.

The D_2 structures have a clear heterogeneous distribution, being mostly concentrated in the vicinity of discontinuous NNE-SSW sub-vertical structures. These planar anisotropies define elongated narrow domains where the regional D_1 NNW-SSE trend were rotated anticlockwise towards WNW-ESE (Fig. 6) defining a mappable D_2 NNE-SSW sinistral kink bands geometry (Fig. $8A_1$ and A_2: Dias *et al.,* 2016b). The transcurrent kinematics is confirmed by several slip evidences like subhorizontal groove lineations (Figs. $8A_3$ and A_4) coupled with the predominance of the minor sinistral kink-bands with high dipping D_2 hinges (Fig. $8A_2$ and A_5).

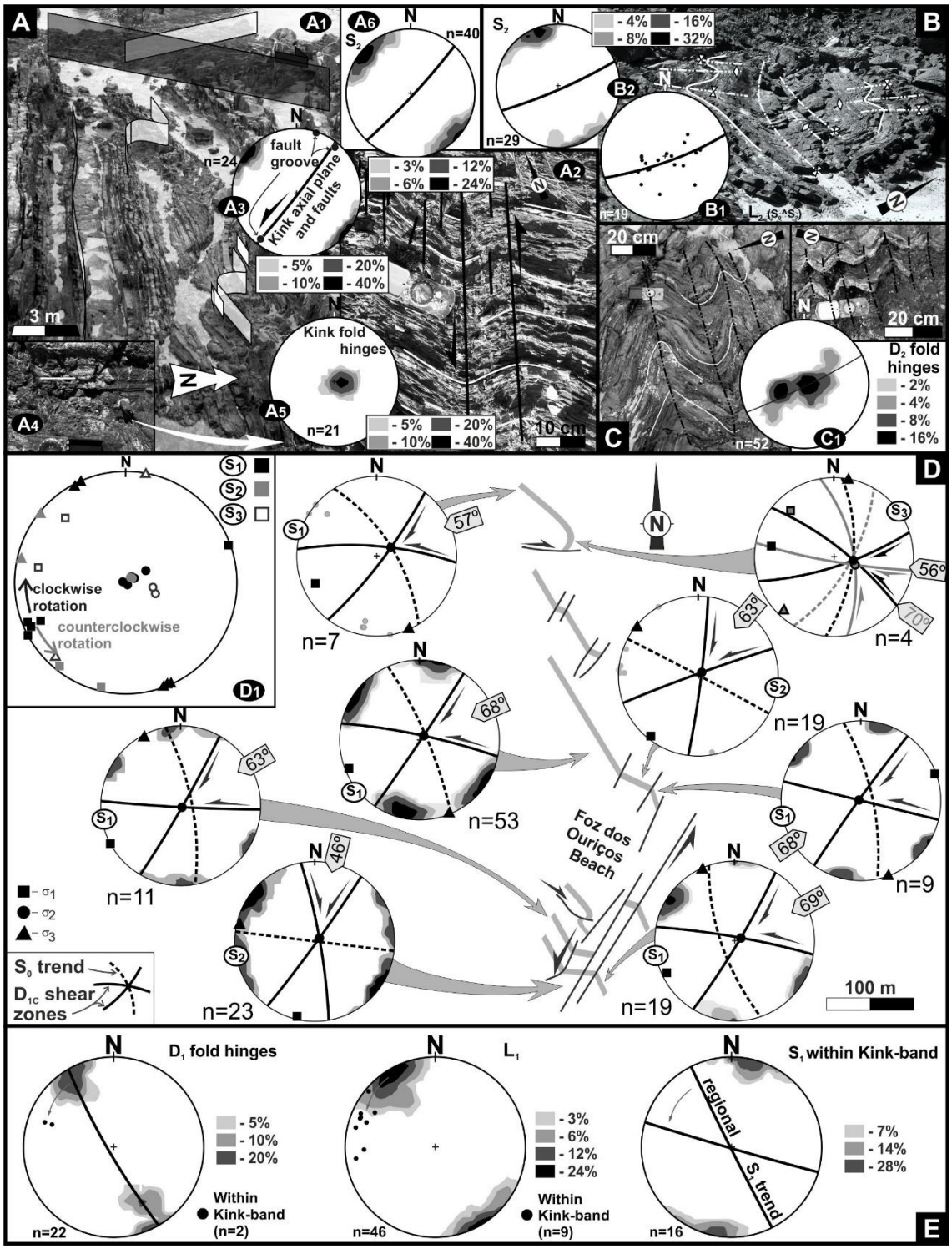
A
A1
A6
S2
N
n=40
n=24
fault groove
Kink axial plane and faults
A3
- 3% - 12%
- 6% - 24%
A2
- 5% - 20%
- 10% - 40%
3 m
Kink fold hinges
A5
n=21
A4
Z
10 cm
B
S2
- 4% - 16%
- 8% - 32%
B2
n=29
n=19
B1
L2 (S1^S2)
20 cm
C
n=52
C1
D2 fold hinges
- 2%
- 4%
- 8%
- 16%
D
S1
S2
S3
clockwise rotation
counterclockwise rotation
D1
57°
n=7
56°
70°
63°
n=4
68°
n=53
n=19
63°
n=11
Foz dos Ouriços Beach
68°
n=9
46°
n=23
69°
n=19
100 m
σ1
σ2
σ3
S0 trend
D1c shear zones
E
D1 fold hinges
- 5%
- 10%
- 20%
Within Kink-band (n=2)
n=22
L1
- 3%
- 6%
- 12%
- 24%
Within Kink-band (n=9)
n=46
S1 within Kink-band
regional S1 trend
- 7%
- 14%
- 28%
n=16

Figure 8 – D_2 sinistral kink bands and its interference with previous D_1 structure (equal area lower hemisphere stereographic projections):

A – Bedding deflection at distinct scales (A_1 and A_2) induced by D_2 sinistral NNE-SSW kink bands (A_3). Sub-horizontal groove lineations (A_3 and A_4), subvertical D_2 fold hinges (A_5) and NE-SW en-echelon cleavage are compatible with sinistral kinematics (A_6)

B – D_1 fold refolded by D_2 with coeval development of L_2 intersection lineation (B_1) and S_2 cleavage (B_2).

C – Orthorhombic D_2 folds with high scatter of fold hinges (C_1) due the interaction with D_1 structure;

D – Rotation of late D_1 conjugate shear zones directions inside the D_2 kink bands;

E – Similar counterclockwise rotation exhibited by D_1 fold hinges, L_1 and S_1 structures within sinistral D_2 NNE-SSW kink bands.

The interference between the progressive coaxial D_1 deformation with the non-coaxial D_2 event produces a complex finite deformation. As the D_1 and D_2 axial planes have sub-perpendicular trends and they are both sub-vertical, a type 1 interference fold pattern was generated (Ramsay e Huber, 1987). Thus, the geometry of the D_2 folds is strongly conditioned by the geometry of previous D_1 folds, with the plunge of the D_2 axes controlled by the geometry of the D1 folds (Fig. 8B). These D_2 folds, are developed near the kink band boundaries, usually presenting an orthorhombic symmetry (Fig. 8C), develop an incipient axial planar S_2 crenulation cleavage (Fig. $8B_2$), generally restricted to fine-grained lithologies. Such geometrical relation give rise to a L_2 intersection lineation (S_0^S_2) subparallel to D_2 hinges (Fig. $8B_1$ and $8C_1$). The axial planes of these orthorhombic D_2 folds are subparallel to slightly oblique (NE-SW) in relation to the NNE-SSW kink planes; this angular discrepancy is compatible with the sinistral kinematics emphasized by the major kink folds (Fig. 6). Such regional left lateral strike-slip component along the NNE-SSW trend has also been emphasized in SW Portugal by en-echelon NE-SW D_2 folds transected by an ENE-WSW S_2 cleavage (Caroça and Dias, 2002).

The conjugate shear zones developed in the late stages the D_1 (Fig. 7C) had also been counter clockwise rotated by the D_2 kink bands (Fig. 8D), showing once more the later development of the kink band structures. The amount of rotation in the inner domains of the kink bands is proportional to the deflection exhibited by the other D_1 structures (S_0, folds in L_1 and S_1; Fig. 8E) ranging from 30 to 60º.

Although the predominant decametric Late Variscan structures in Almograve are the sinistral NNE-SSW kink bands, locally E-W to WNW-ESE kink-like folds are developed (Figs. 6 and 9). They also present a brittle-ductile behavior, underlined by frequent quartz veining and

the common disruption of bedding. Their dextral kinematics is shown by the rotation of previous structures, with the related D_2 folds presenting E-W axial planes and highly plunging hinges (Fig. 9).

The coeval development of these E-W dextral kink-bands with the NNE-SSW sinistral ones is proven by the mutual interferences between structures from both sets (Fig. 6), also rotating the late D_1 conjugate shear zone, in this case with clockwise rotation (Fig. 8D).

Similar dextral E-W kink band, attributed to the Late Variscan stage, have been described along the SW Portuguese coast (Dias and Basile, 2013; Dias et al., 2016b).

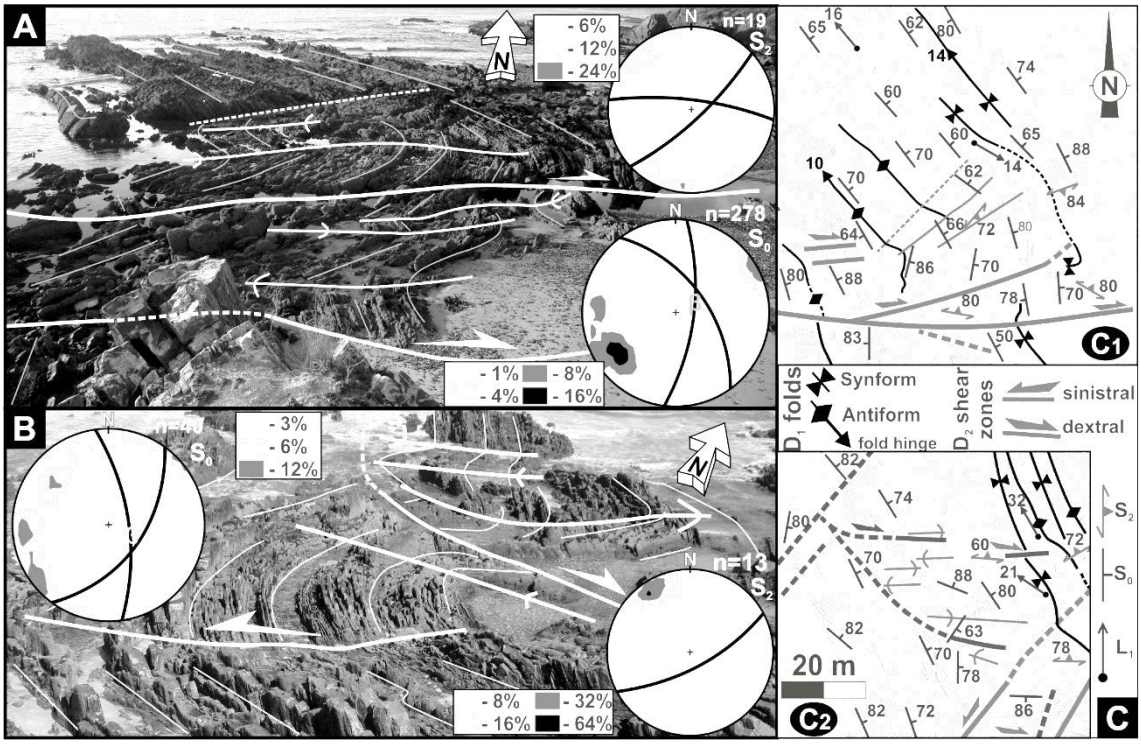

Figure 9 – E-W dextral D2 shear zones (equal area lower hemisphere stereographic projections of S_0 and S_2):

A – Kink-like fold generated by D_2 dextral shear along E-W fault in northern sector;

B – Complex interference between NE-SW kink bands and E-W dextral shears in the southern;

C – Structural map of A (C_1) and B (C_2) domains.

Occasionally closely spaced D_2 conjugate kink bands are developed giving rise to box-folds (Fig. 10), with subvertical to high dipping axial planes and hinges. The shape of the folded layers allows to distinguish two kink band families: the sinistral with a NE-SW trend and the dextral ESE-WNW to E-W one. In the shale rich turbiditic sequences the angle between both families ranges between 55º to 90º (Fig. 10A), while when the greywackes are predominant such angle tends to be smaller (34º; Fig. 10B).

As expected, the space problems related to the quasi-rigid rotation inside the D_2 kink bands, led to the development of accommodation structures. In the NNE-SSW kink bands, the bedding rotation from the regional NNW-SSE to WNW-ESE (Fig. 6), induced in the internal domain a pervasive dextral shearing along the bedding planes giving rise to a diversity of minor structures (Fig. 11; Dias et al., 2016b). The most evident are D_2 asymmetric folds (Fig. 11A) with subvertical to high plunging hinges (Fig. $11A_1$) and subvertical NE-SW axial plane S_2 cleavage (Fig. $11A_2$). In the long limbs of these folds subhorizontal to gently plunging slickensides (> 30º) are often found (Fig. 11B), enhancing the transcurrent kinematics. The dextral shearing is also supported by other structures like sigma shape competent bodies of greywackes inside non-competent shales (Fig. 11C) or dextral shear zones with trends close to ENE-WSW (Fig. 11D). Although less important, also NW-SE sinistral brittle to brittle-ductile shears zones were developed (Fig. $11D_1$), showing a WNW-ESE σ_1 compatible with the dextral shearing pervasive in the kink band. Locally, NW-SE dextral shear zones are developed (Fig. 11E), being geometrically compatible with C' shears bands of the main WNW-ESE dextral layer parallel shearing within kink-band.

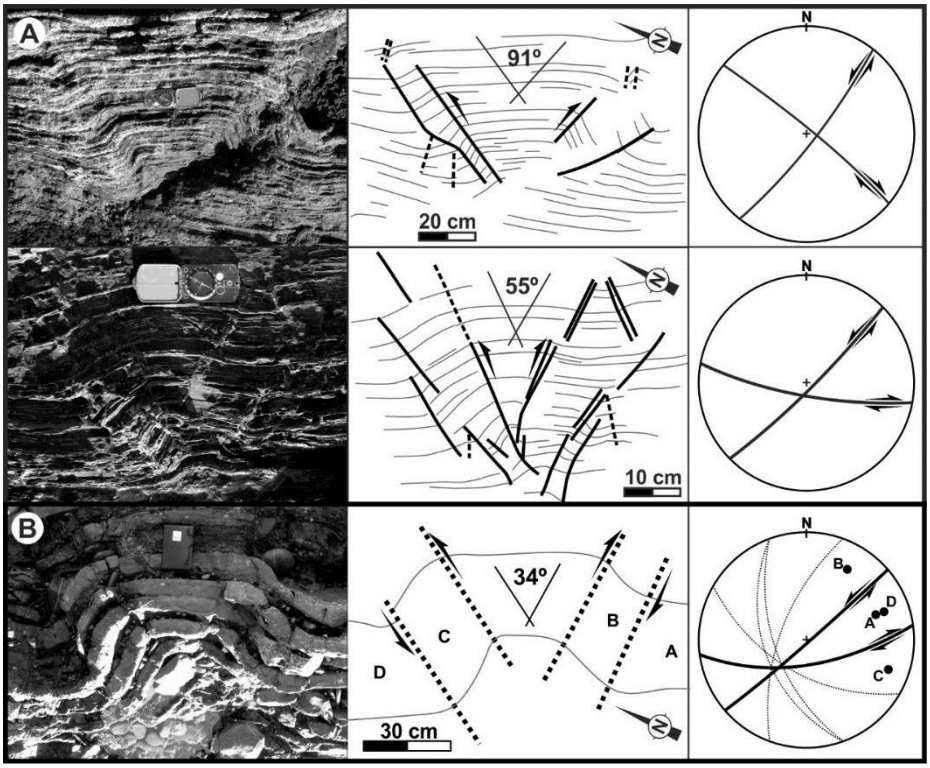

Figure 10 – Geometry and kinematics of D_2 conjugate kink bands inducing box fold geometries in (equal area lower hemisphere stereographic projections of axial planes):

A – Shale rich sequences;

B – Greywacke rich sequences.

Near the kink band boundaries some D_1 subvertical boudins were reworked, generating NE-SW sinistral shear zones (Fig. 11F), which is kinematically compatible with the sinistral shearing of the regional NNE-SSW kink bands.

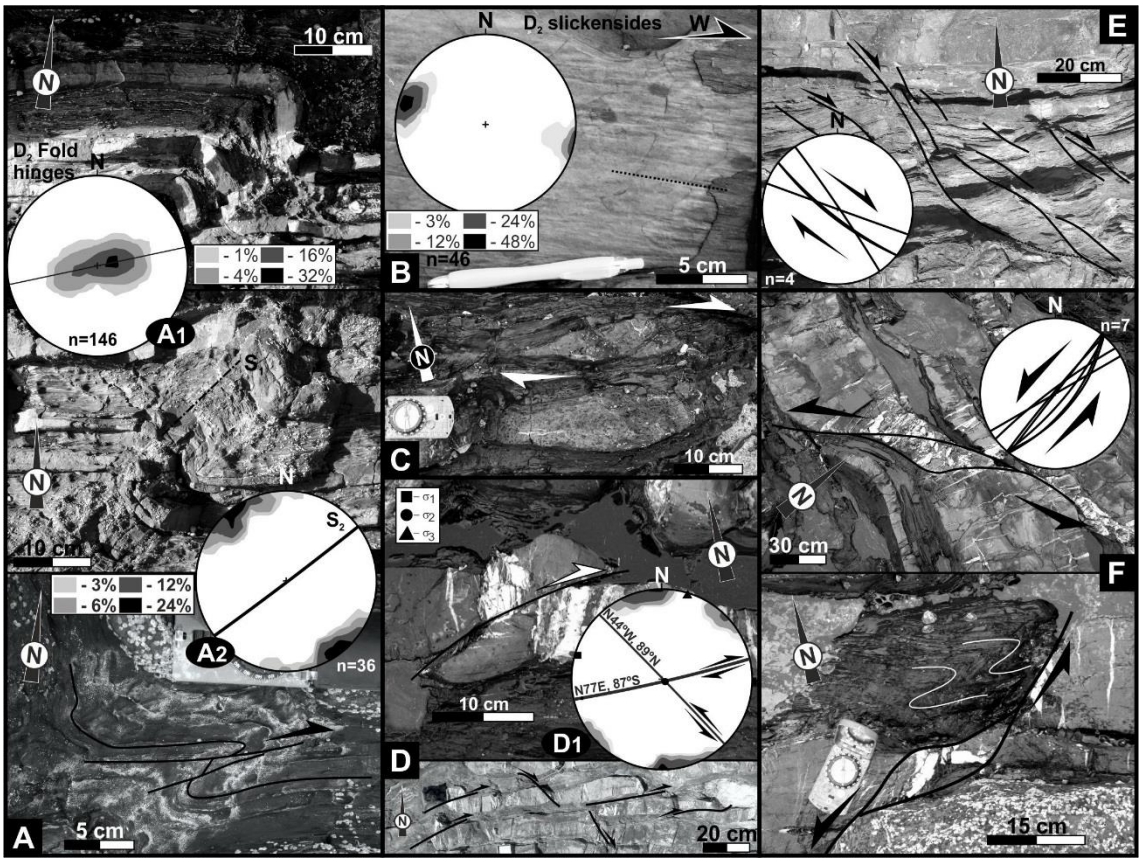

Figure 11 – D_2 structures developed within the NNE-SSW sinistral kink bands (equal area lower hemisphere stereographic projections):

A – Flexural asymmetrical folds with subvertical hinges (A_1) and a NE-SW cleavage (A_2);

B – Sub-horizontal slickensides;

C – Sigmoidal greywacke body developed in a shale-rich turbidite;

D – Dextral shear zones affecting greywacke beds and related stress field obtained using the conjugated sinistral shear (D_1);

E – Dextral NW-SE shears compatible with a C' geometry;

F – Sinistral NE-SW shears developed in a D_1 boudin necks.

X.2.4.2. Abrantes Kink Band

The Abrantes region is located in the northwestern sectors of Ossa-Morena Zone (Fig. 5B) where a Neoproterozoic-Cambrian lithostratigraphic sequence is found (Moreira et al., 2015). These formations were deformed by two ductile Variscan deformation phases (D_1 and D_2) prior to the Late Variscan brittle to brittle-ductile event. As in Almograve the Late Variscan event

induces the formation of mesoscopic kink bands due to the rigid rotation of previous planar anisotropies. However, in Abrantes the deformation of the metasediments, older than the Late Variscan, is stronger than in Almograve, which reflects the position in the orogen: the Ossa-Morena Zone is contained in the highly deformed orogenic hinterland, while the South Portuguese Zone represents the less deformed orogenic foreland (Ribeiro et al., 2007; Moreira et al., 2014).

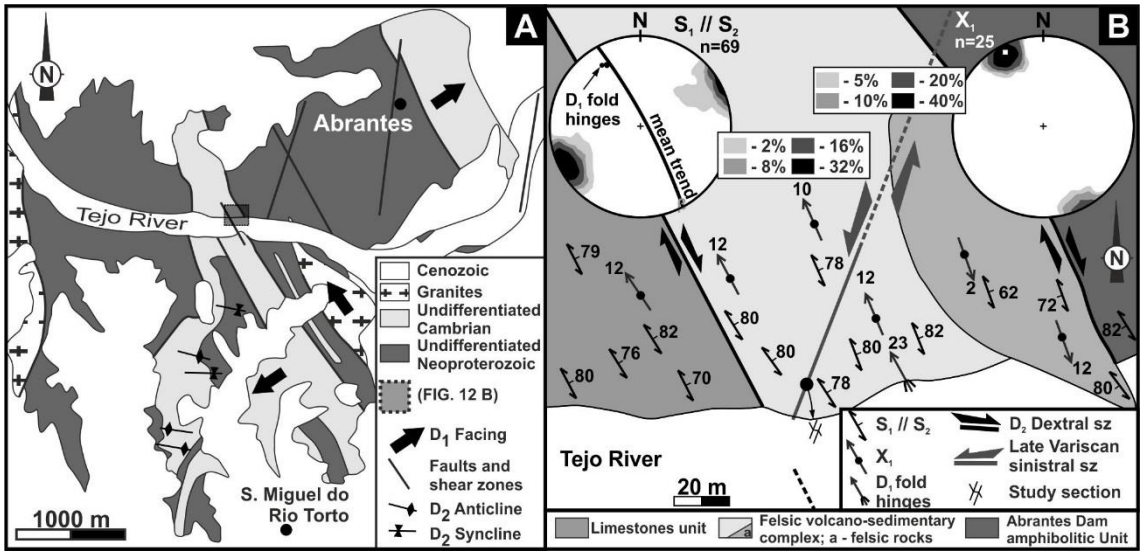

Figure 12 – Geological setting of Abrantes kink band:

A – Simplified geological map of Abrantes region (adapted from Moreira, 2012);

B – Structural map and Schmidt diagrams (equal area lower hemisphere stereographic projections) of early Variscan events, with localization of the studied kink band.

The first deformation episode (D_1), related to a medium grade foliation, generates a complex folded structure with a NNW-SSE trend. Indeed, in an axial zone there is tangential transport to NW, while the facing in the NE sector is towards NE and in SW it is to SW (Fig. 12A). Such pattern has been considered the result of a kilometric D_1 sheath fold associated with the north-west termination of the sinistral Tomar-Badajoz-Cordoba shear zone (Fig. 5B; Ribeiro et al., 2007; Moreira, 2012).

The second deformation phase (D_2) is associated with a right-lateral non-coaxial regime along the NNW-SSE orogenic trend. The D_2 distribution is highly heterogeneous with domains where WNW-ESE folds are predominant (Fig. 12A) juxtapose to others mainly affected by NNE-SSW dextral shear zones. Such pattern was considered due to a strong strain partitioning in a general NNE-SSW dextral transpressive regime (Moreira, 2012). The intensity of D_2 increases westwards towards the dextral Porto-Tomar-Ferreira do Alentejo shear zone (Fig. 5B), which

led to consider that the movement along this first order transcurrent shear zone was responsible by the D_2 episode in this sector (Romão et al., 2014; Moreira et al., 2016).

In the studied area (Fig. 12B), the structure is characterized by a NNW-SSE subvertical to strongly dipping to NE foliation. This foliation, where a sub-horizontal stretching lineation is observed (Fig. 12B), is mostly the result of the D_1 episode, although strongly reworked by the D_2 dextral shearing.

The Late Variscan deformation induces in the Abrantes region a set of subvertical D_3 structures (faults, fracturing, quartz veins, and kink bands; Fig. 13), with NE-SW to NNE-SSW trends (Figs. 13A, 13C and 13D). These structures are often related with quartz veins and cataclasis, which sometimes also affects the quartz veins (Fig. 13B), enhancing their brittle to brittle-ductile behaviour. Either the offsets of previous markers along centimetric faults (Fig.13C), or the geometry of kink bands (Fig. 13D) shows clear left-lateral kinematics along the NE-SW trend.

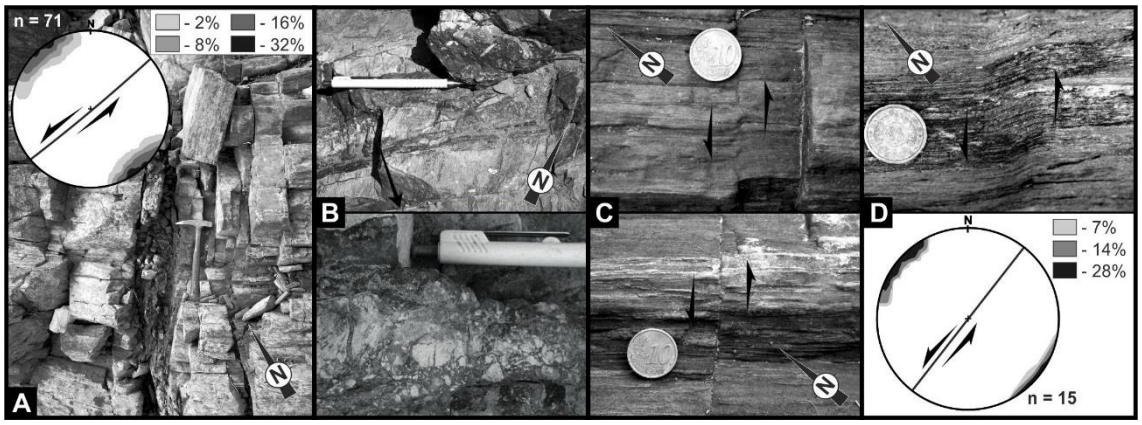

Figure 13 – Late Variscan structures in Abrantes region:

A – Intense fracturing associated to NE-SW mesoscopic fault (equal area lower hemisphere stereographic projection of main fractures);

B – Mesoscopic fault underlined by quartz veining and cataclasis;

C – Centimetric sinistral offsets in NE-SW faults;

D – Centimetric sinistral kink band and geometric behaviour of similar structures (equal area lower hemisphere stereographic projections).

The kink-bands, with a millimetric to a metric scale, are more common in the silica-rich felsic volcano-sedimentary complex where the S_1 foliation is well developed. The study of one of the metric kink band (Fig. 12A and 14) led to a better understanding of the mechanisms related to its formation. This N20ºE to N30ºE subvertical structure deflect previous planar structures (S_1//S_2) from the NNW-SSE regional trend to ENE-WSW.

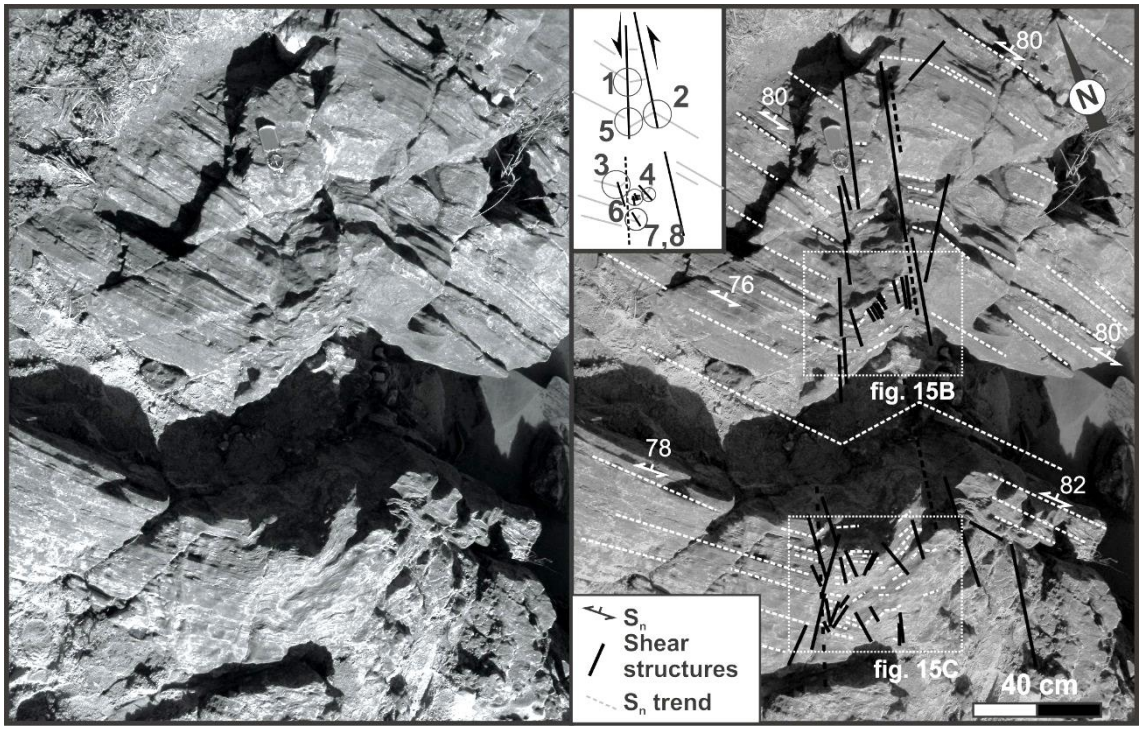

Figure 14 – General pattern of sinistral Abrantes metric kink band.

The boundaries of the Abrantes kink band are complex (Fig. 14), which could indicate it was due to the coalescence of small linear segments separated by steps or relays as proposed by Peacock and Anderson (1995) to strike slip faults. Inside the kink band a pervasive array of subvertical 2nd order fractures, was developed (Fig. 15). The trend of these fractures shows two main sets (Fig. 15A): the main set has a very consistent N-S orientation (±3º, 95% confidence interval), while the second one, is less developed and presents some dispersion around a mean N55ºE average direction (±14º, 95% confidence interval). Nevertheless, the two sets show clear evidences of rigid rotation of the previous anisotropy (S_1//S_2) inside a pair of planar structures (Fig. 15B and 15C). Such rotation generates folds with straight limbs and sharp hinges, acting as 2nd order kink bands. The geometry of both sets shows distinct kinematics: the N55ºE trend shows a pervasive clockwise (dextral) rotation while the N-S orientation generally have a counterclockwise (sinistral) rotation. Thus the N-S set is synthetic in relation to the main NNE-SSW kink band kinematics, while the N55ºE one is antithetic. Nevertheless, when a large amount of N-S structures are developed, a symmetric pattern tends to occur (Fig. 15B1). When both sets are closely spaced box-folds geometries are developed (Fig. 15B2 and 15C).

As usually, often the kink band planes of Abrantes show evidences of some slip leading to the sinistral disruption of previous planar foliation (Fig. 15C1).

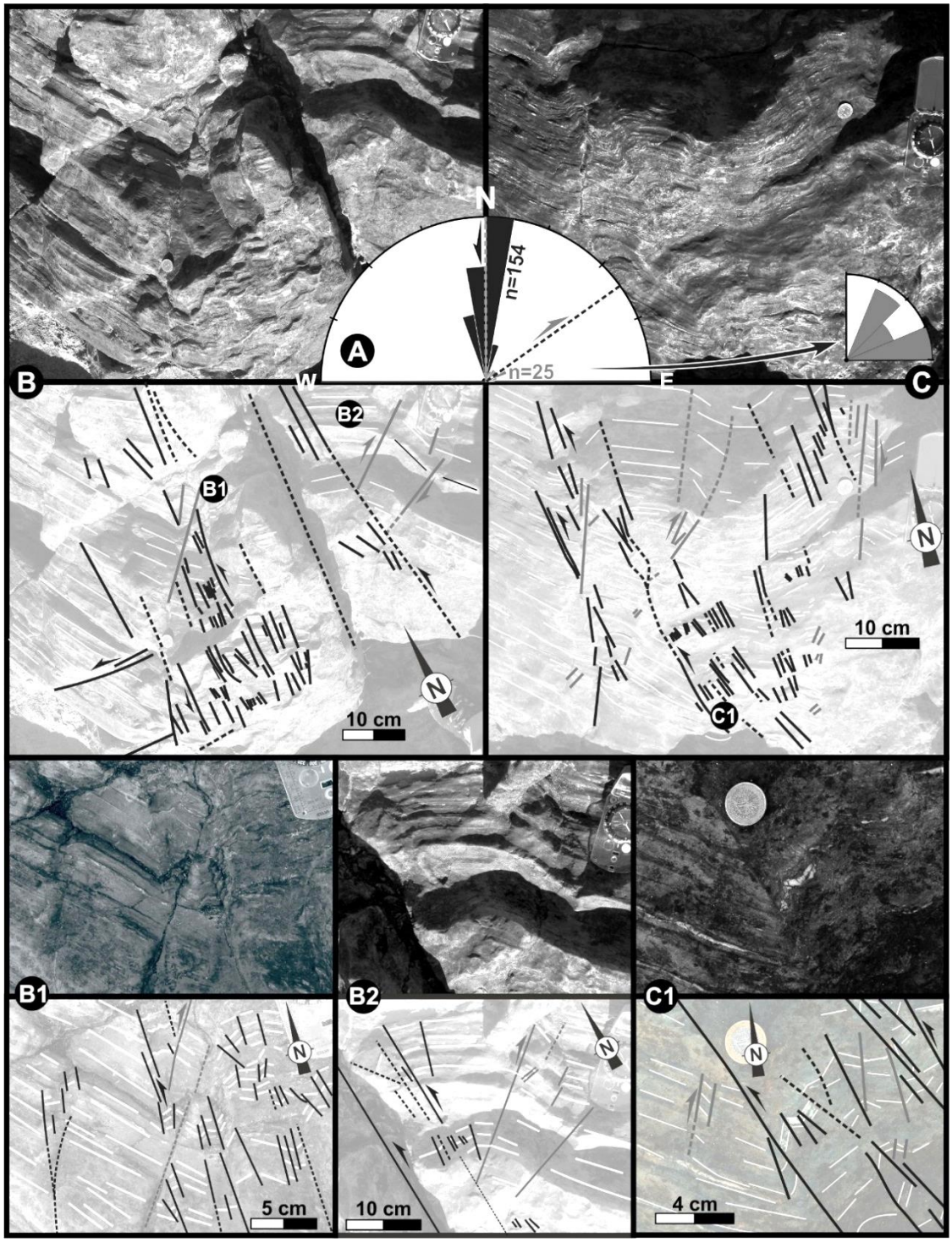

Figure 15 – Main geometric and kinematical features of Late Variscan Abrantes kink band fracture pattern:

A – Rose diagram of 2nd order kink bands;

B – Predominance of sinistral N-S fractures, with symmetrical shape in highly deformed sectors (B1) and local box folds development (B2).

C – Diffuse boundaries of Abrantes kink band, sometimes showing offsets of previous layered structures (C1).

X.2.4.3. Stress Analysis in Almograve and Abrantes Kink Bands

The Almograve and Abrantes kink bands geometry support the sinistral kinematics of the Late Variscan NNE-SSW faults. Nevertheless, they have distinctive features which seems to result mainly from the rheology of the affected formations.

In Almograve, the stress field of the Late Variscan kink bands was estimated using the bisector method (Stewart and Alvarez, 1991) in three sectors where conjugated kink bands are found. All are located outside the major mesoscopic kink band where the D_1 structures have the regional NNW-SSE trend (Fig. 5). Thus the obtained stress fields have a regional meaning because they have not been rotated during the kink band formation. In all cases the intermediate tensor (σ_2) is subvertical, while the maximum (σ_1) and minimum (σ_3) tensors are subhorizontal, with NNW-SSE and ENE-WSW directions respectively (Fig. 16A_3). The angular relation between the σ_1 direction and the primary layering (α), although very small shows positive (i.e. the σ_1 acting in the clockwise side of the primary layering; Fig. 16A_1), or negative (Fig. 16A_2) values. The negative α were obtained near the NNE-SSW sinistral kink bands, showing that they induce a slight counter clockwise rotation of σ_1, synthetic with the rotation of primary layering within the kink band. If is it considered the mean directions of cartographic scale dextral and sinistral kink bands (Fig. 6), similar stress field is obtained: σ_1 and σ_3 contained in horizontal plane, respectively with N30ºW and N60ºE direction and σ_2 subvertical (Fig. 16A_4).

Within Almograve kink bands the shortening of the layers related to their rotation, induced in the more competent layers conjugated shear zones. Their stress field (Fig. 16B) also have subhorizontal σ_1 and σ_3 (respectively 04º, N73ºW and a 01º, N16ºE attitude) and subvertical σ_2 (86º, S57ºE). This internal stress field related to the evolution of the kink band, is counter clockwise rotated in relation to the previous stress fields (Fig. 16A) which are typical of the external domains. Thus, the obtained stress field could be interpreted as related to layer-parallel shortening within kink-band.

In the Abrantes kink band, the internal stress field was obtained using the 2nd order conjugate kink bands developed within kink band. The stress field presents subvertical σ_2 and subhorizontal σ_1 and σ_3 (Fig. 16C), respectively with a WNW-ESE and a NNE-SSW trends. Such stress field is also compatible with the layer parallel shortening during the rotation process.

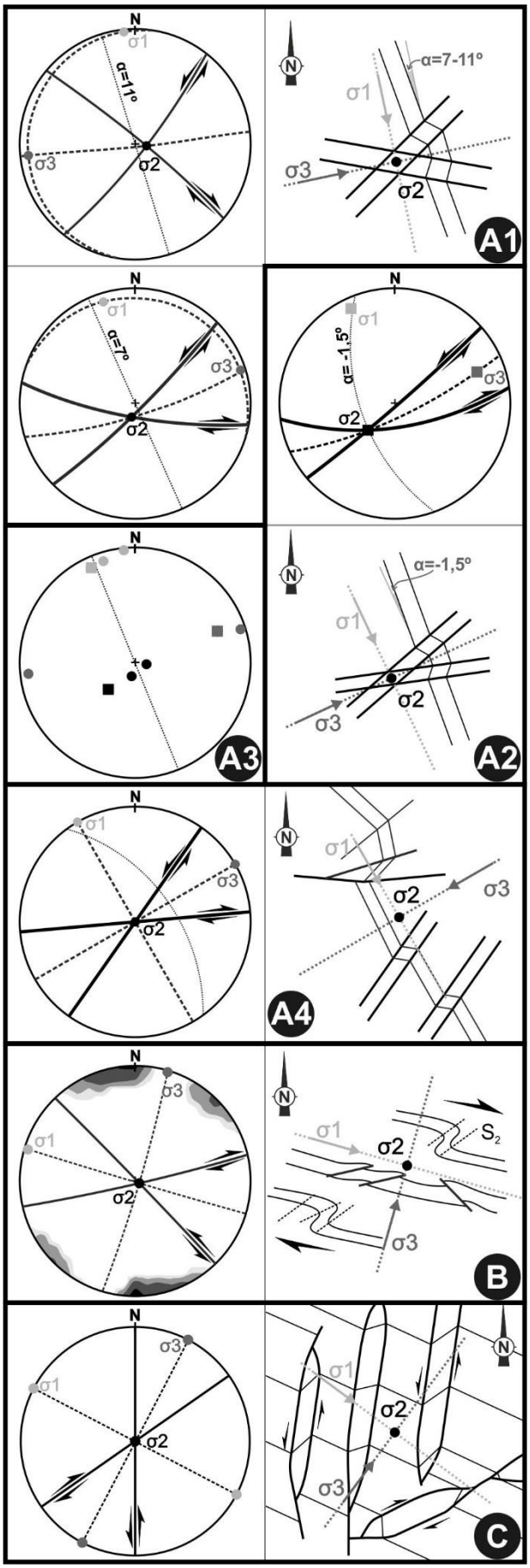

Figure 16 – Stress field analysis based on D_2 structures:

A – External NNW-SSE domains of Almograve kink bands, based on D_2 kink bands. Similar stress field was obtained based on cartographic scale structures (A_4);

B – Internal WNW-ESE domain of major Almograve kink band, based on D_2 conjugate shear zones;

C – Internal stress field of Abrantes kink band data using 2nd order kink-bands.

Although the stress fields obtained for the Late Variscan kink bands are similar for Almograve and Abrantes, the induced structural patterns originated by rotation and consequent layer parallel shortening are quite different (Fig. 16B and 16C). Flexural folds were formed in both cases, but they present distinct shapes due to the different rheology of the deformed multilayers. Indeed, in Almograve the folds were formed by dextral shear slip between adjacent layers (Fig. 11A) induced by the internal kink band rotation. The coeval layer parallel shortening was expressed, either by conjugate shear zones developed in the competent greywacke layers, or by orthorhombic folds found near the kink band boundaries (Dias et al. 2016b). In Abrantes, the layer parallel shortening on homogeneous lithological successions generates 2nd order conjugate kink bands.

X.2.5. Shortening Quantification in Almograve and Abrantes Kink Bands

The frequent complex structural pattern of kink bands and the existence of different genetical processes difficult the estimation of the shortening induced by rotation during their formation. However, when the genetical mechanism is known, it is possible to approach such distortion.

The projection of angular values of Abrantes and Almograve kink bands (table II) in the Srivastava et al. (1998) triangular diagram (Fig. 17), shows the clear predominance of the fixed hinge mechanisms (type III). Such classification is compatible with the field data for both regions, where their boundaries seem to have been stable during the deformation, sometimes with evidences of simple shear along boundaries. The presence of shortening structures within kink band and the occurrence of interlayer slip in Almograve are also evidences of type III model. The dispersion of data towards type IV model could indicate, either a slight change of the kink band boundaries during layering rotation, or the variation of angular parameters during the deformation process, as could happen by layer parallel slip on internal foliation (Stewart and Alvarez, 1991).

Previous works developed a graphical method to evaluate the volume variation within kink bands (Dewey, 1969; Suppe, 1985). Such approach was adapted to fixed hinge type III model assuming the geometrical constraints typical of this model (Fig. 18). The shortening quantification assumes that the kink band boundaries are parallel and kink band width (W) remains invariable during the rotation of internal primary layering. During the deformation progress, the length of primary layering from its initial position (L_0) to its final position (L_1) varies, allowing the shortening measure (Fig. 18). During rigid rotation, the angular values relation presents variations, always obeying to equation 1.

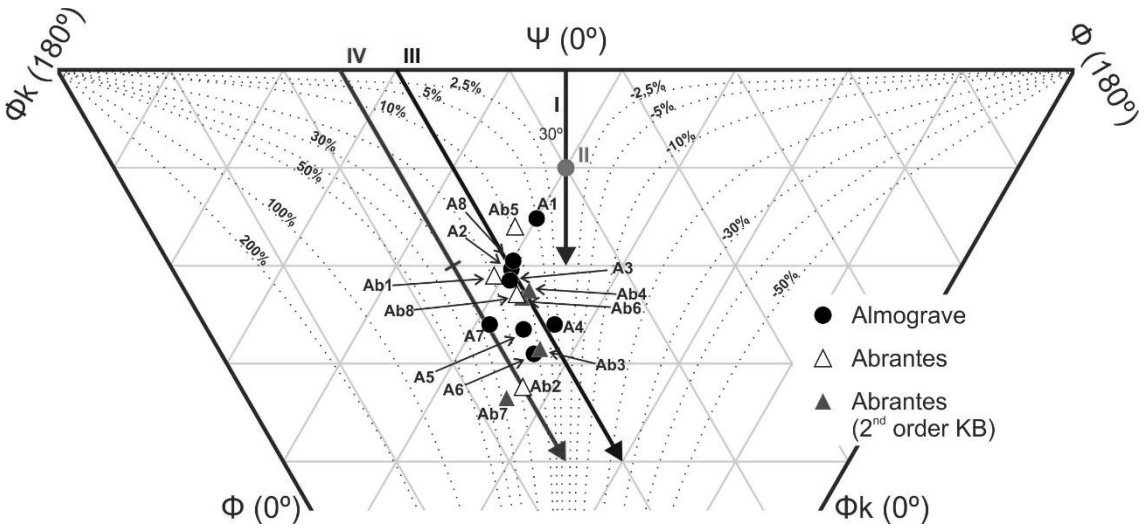

Figure 17 – Almograve and Abrantes data in Srivastava et al. (1998) triangular graphic of kink band types.

Table II – Angular parameters of Almograve and Abrantes kink bands (locations in figures 6 and 14).

		Φ	Φk	Ψ	Model type
Almograve	**A1**	69,5	80,5	30	near III
	A2	60	79	41	III
	A3	58,5	78,5	43	III
	A4	62	**66**	52	III
	A5	56	**61**	63	III
	A6	55,5	**66,5**	58	III
	A7	**50,5**	**67,5**	62	IV
	A8	61	80	39	III
Abrantes	**Ab1**	57,5	80,5	42	III
	Ab2	**50**	**65**	65	IV
	Ab3*	57	**66**	57	III
	Ab4*	61	74	45	III
	Ab5	65	83	32	near III
	Ab6*	59	74,5	46,5	III
	Ab7*	**47**	**66**	67	IV
	Ab8	58	76	46	III

* - 2nd order kink band

It was generated a predictive model based in a point matrix generated by multiple interactions for ϕ and ϕk angular values during the rotation. Associated with each (ϕk,ϕ) quoted point it was measured the stretching value ($S = L_1 / L_0$). All quoted points and respective S value are projected in bivariate graph, being generated a predictive model using the ordinary kriging as spatial interpolation method (Fig. 18A). When the ϕ angle is smaller than 30º a new kink band is not generated, since the shear reactivation of inhered primary layering are pervasive (Sibson, 2012).

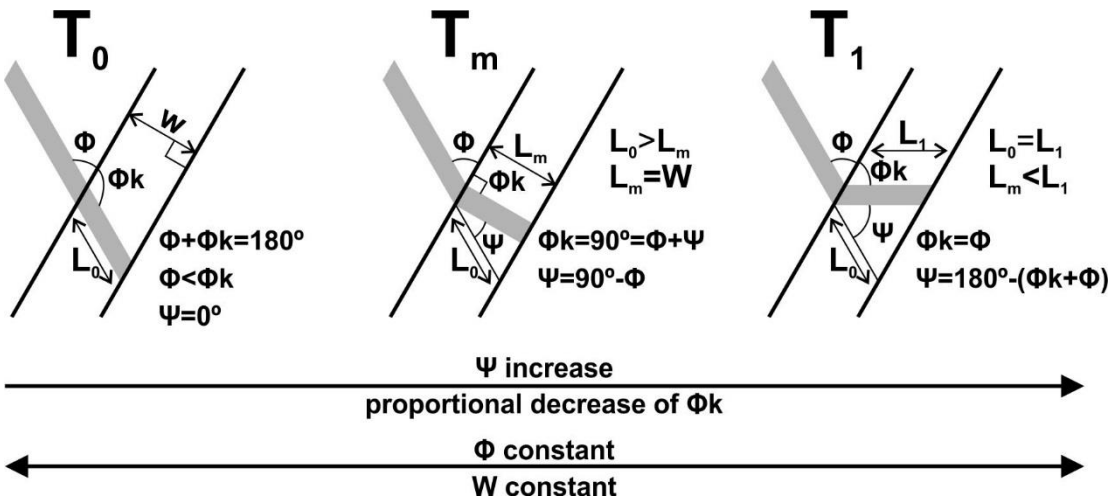

Figure 18 – Summary parameter conditions for graphic construction. Stretching parameter was obtained with the variation of length during rotation with constant kink-band width.

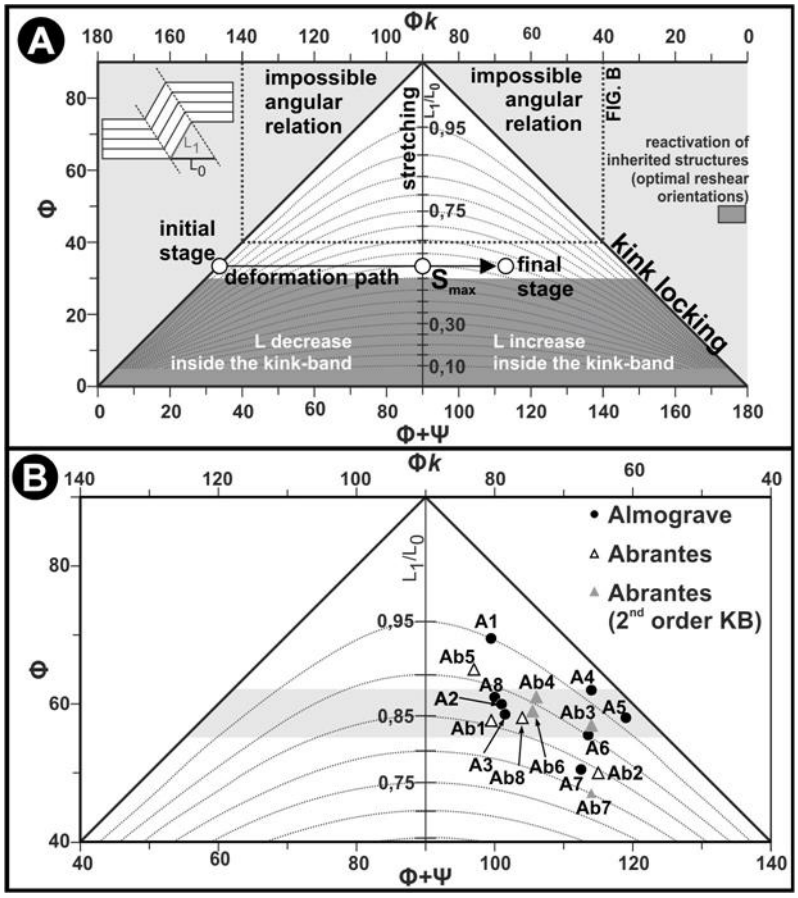

Figure 19 – Graphical estimation of stretching in type III fixed-hinge kink bands:

A – Proposal graphical method for shortening kink band analysis. The arrow represents an example of evolution of a kink band;

B – Projection of Almograve and Abrantes kink bands.

The use of this method in Almograve and Abrantes kink bands indicates a shortening ranging from 6 to 26% (Fig. 19B; table III). The projection of the data in the $\phi k > \phi$ field with $\phi k < 90º$ indicates a strong rotation of the kink bands during deformation, although lower than the theoretical maximum rotation (i.e. $\phi k = \phi$). The lower values of shortening is proportional to higher ϕ values, because the rotation until the orthogonal position is smaller.

Table III – Shortening values for Almograve and Abrantes kink bands (locations in figures 6 and 14).

		S max	Maximum shortening (%)	S actual position	S component (%)	$S_{\perp}$ Stewart and Alvarez (1991)
Almograve	**A1**	0,936	**6,4**	0,950	1,4	1,06
	A2	0,866	13,4	0,882	1,6	1,13
	A3	0,853	14,7	0,871	1,8	1,15
	A4	0,884	11,6	0,967	**8,3**	1,03
	A5	0,829	17,1	0,953	**12,4**	1,05
	A6	0,824	17,6	0,902	**7,8**	1,11
	A7	0,772	**22,8**	0,834	**6,2**	1,19
	A8	0,875	12,5	0,888	1,3	1,13
Abrantes	**Ab1**	0,843	15,7	0,855	1,2	1,17
	Ab2	0,766	**23,4**	0,845	**7,9**	1,18
	Ab3*	0,839	16,1	0,923	**8,4**	1,09
	Ab4*	0,875	12,5	0,910	3,5	1,10
	Ab5	0,906	**9,4**	0,913	0,7	1,10
	Ab6*	0,857	14,3	0,890	3,3	1,12
	Ab7*	0,732	**26,8**	0,803	**7,1**	1,25
	Ab8	0,848	15,2	0,875	2,7	1,14

These data emphasize some heterogeneity of the deformation. Indeed, in the Almograve main kink band (Fig. 6), four different shortening values were obtained (A4 to A8; Table III) ranging between 12% and 23%. This scatter could result from distinct displacements in the central and bordering areas of the same kink, which is compatible with lower shortening values closer to the boundaries where the rotation was smaller. However, the dispersion could also result from variation of ϕ values during deformation, like their decrease due to discrete slip along kink band boundaries. Evidences of sinistral slip along the boundaries are found both in Almograve (A7 kink band; Fig. 8A) and Abrantes kink bands (*e.g.* Ab7 kink band; Fig. $14C_2$).

Indeed, the three kink bands with higher values of shortening (A7, Ab2 and Ab7) fall in type IV field (Fig. 17), suggesting variation of ϕ during deformation. Concerning the obtained lower values of shortening (A1, A4 and Ab5) could be related with the increase of ϕ due to layer parallel slip in the external domains of the kink bands as already suggest (Stewart and Alvarez, 1991). In fact, there is evidences of slip in outer domains of kink band near A4 kink band, due the action of dextral shear related to kink-like fold (Fig. 6).

The Almograve and Abrantes kink bands always present ϕk lower than 90º which, for fixed kink boundaries, indicates that they already initiate a process of layer-parallel stretching (Fig. 19B). Nevertheless the extension rate in most cases is very small, (*i.e.* S component lower than 5%; table III), which means that some kink bands is almost orthogonal to kink band boundaries. Although in both regions the structural evidences of stretching within kink bands are not common, some localized C' shear zones in Almograve are compatible with layer parallel stretching (Fig. 11E). However, some care should be taken, because ϕk angle could also decrease due to slip of internal layering (Stewart and Alvarez, 1991), as sometimes observed in Almograve kink bands (Fig. 11A and 11B).

The strength of previous methodology could be accessed by comparing the graphical estimations with values obtained by independent approaches. In Abrantes, a thin quartz vein parallel to the main planar anisotropy and with a Ψ=46º (Fig. 20A_1; Ab8 sample) were reconstructed to its linear undeformed state (Fig. 20A_2). The comparison between the initial and final lengths shows that the kink band induced a 18% of shortening of the structure, which is quite similar to the 15,2% obtained by the graphical method and with the general range obtained to Abrantes type III kink-bands (13 to 17%; Table III). The widespread development of 2nd order conjugate contractional kink bands displacing the internal layering (Fig. 15B_2), shows that this shortening parallel to the layering was compensated by stretching in the orthogonal direction without evidences of vertical escape.

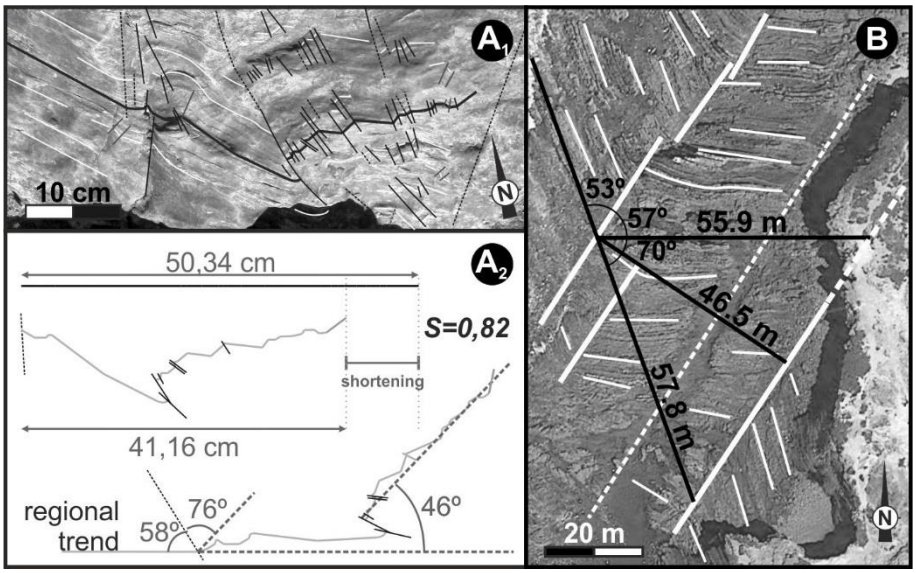

Figure 20 – Shortening estimation of kink band real cases:

A - The general pattern of Abrantes kink band (sample Ab8) using a quartz vein parallel to layering as strain marker (A_1) and the parameters used in the finite quantification (A_2).

B– General pattern and geometrical parameters of Almograve kink band.

Also in Almograve, the shortening was deduced by the geometry of a well exposed wave cut platform sinistral main kink band (Fig. 20B). Here, the total rotation ranges 70º and the maximum shortening is also circa of 19%. Taking into account the angular values (Fig. 21A), the proposal graph methodology estimate 20% of shortening. This value fits the Almograve estimations using the graphical approach that gave a maximum shortening usually ranging between 13 and 18% (table III and Fig. 19B).

The compatibility between the shortening estimations using the graphical methodology and the values obtained by detailed geometrical analysis of two previous examples, shows it is a good approach to estimate the distortion induced by kink band rotation. This is important because this method is fast and easy to use using only the measure of ϕk and ϕ values.

In the horizontal plane of the inner domain of Almograve kink band, several structures were developed due to this shortening. Some of these structures compensate this layer parallel shortening with extension orthogonal to the layering: conjugate shear zones in greywackes (Fig. 11D), orthorhombic folding near kink band boundaries (Fig. 8B) and monoclinic flexural folding due to the dextral reactivation of layering (Fig. 11A). However, the sparse development of these structures are not able to support the overall shortening. Nevertheless, the Almograve kink band is a particular situation where the initial and final lengths are very similar (57.8 m and 55.9 m; Fig. 20B), which give an almost negligible final shortening (*circa* 3%), compatible with the observed structures. Even so, during the intermediate state, where the minimum width was attained (46,5 m; Fig. 20B), some vertical escape is inevitable to compensate the 19% layer parallel maximum shortening. The lack of structures related to this subvertical thickening is due to the outcropping conditions (Almograve is mostly a subhorizontal wave cut platform), and the weakness of the effective stress field related to this subvertical escape.

Thus, it could be assumed a mechanism of rigid rotation of internal layering inside kink band coeval of vertical escape. This vertical variation is able to compensate, either the horizontal layer parallel shortening during the initial stages of kink band formation, or their extension in the latter stages. It should be noted that slickensides plunge also denotes a slightly oblique slip (Fig. 11B), compatible with the presence of a vertical escape component.

The data were also projected in Stewart and Alvarez (1991) graph (Fig. 21A). The data show, as expected, that if the shortening component is applied parallel to the layering, a stretch component is required in other orthogonal direction ($S_{\perp}$ in table III; vertical or parallel to kink band boundaries direction). So, all the Almograve and Abrantes kink bands are projected in $S>1$ field, which means that there is a bulk increase orthogonally to the layering.

The obtained values of streching parrallel and orthogonal to layering through both methods must to be complementar and a negative relationship is require (Fig. 21B). The projection of S_{MAX} vs $S\perp$ shows two distinct clusters are identified (Fig. $21B_1$):

- A1-A3, A8, Ab1, Ab4-Ab8 samples are disposed over or near the proportionality perfect curve (error < 2º), which indicates that both obtained S values are similar;
- A4-A7, Ab2-Ab3 samples are disposed below the proportionality curve (error > 2º) which means that the S component value parallel to layering is higher than the obtained orthogonal one.

The second cluster is coincident with the samples that have highly rotation to beyond the orthogonal position between kink band boundary and internal rotated layering, thus presenting a higher S component (table III). This discrepancy happens because the S_{MAX} parallel to layering is not the finite stretching in the actual position. The linear negative relationship is clearly visible when S in actual position and the S obtained in Stewart and Alvarez (1991) are projected, showing that the proposal method is a good approach (Fig. 21B2). The diference between both comparative graphs (Fig. 21B) corresponds to S component previously mentioned in Table III. The only exception is the sample Ab7, that according our method presents an higher S component. This fact could be related to an angular parameter change, namely decrease in ϕ, related to an intense slip along kink band boundary.

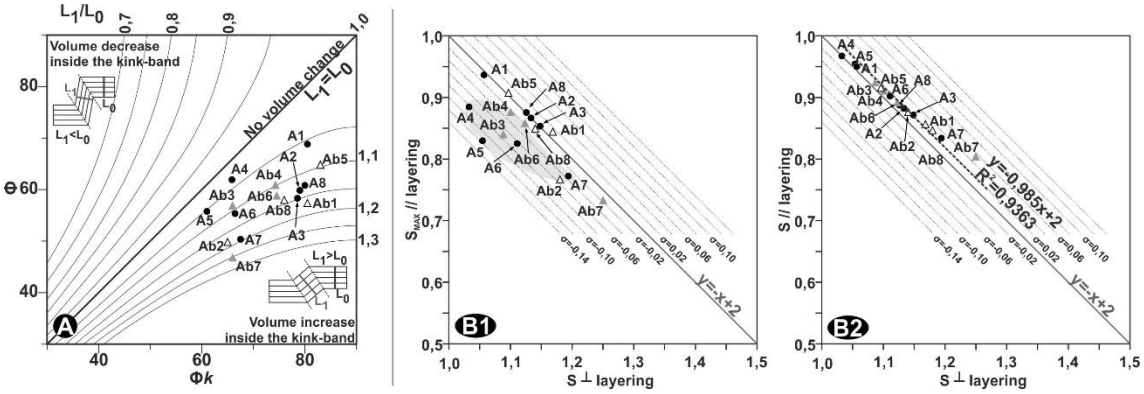

Figure 21 – (A) Thickening variation analysis within kink band using Stewart and Alvarez (1991) graphical method; (B) Comparison between stretching value obtained by proposal method (S // layering) and Stewart and Alvarez (1991) method (S ⊥ layering).

X.2.6. Layer Parallel Shortening and Layer Parallel Slip in Fixed-Hinge Models

The geometric and kinematic features of Almograve kink bands, and their spatial relation with NNE-SSW deformation bands, show this trend have a clear sinistral kinematics during Late Variscan times. The strong distortion induced by the rotation of the inner domain of the kink

band in relation to the outer NNW-SSE regional trend, superimposed on a highly anisotropic sequences, will gave rise to a strong heterogeneous deformation pattern.

In the WNW-ESE domains, the complexity of such deformation is expressed by the coexistence of two different sets of folds. An orthorhombic set of folds is common in the vicinity of sub-vertical kink band boundaries and could be explained by layer parallel shortening. The folds with monoclinic symmetry reflects the relation with dextral layer parallel slip along the subvertical WNW-ESE inner domain. Although both sets of folds are found in the same kink band, their different genetical mechanisms exclude their development in the same place. Nevertheless the absence of interference structures between them are compatible with the same sinistral simple shear along the NNE-SSW trend.

Also the rheology of deformed turbiditic sequences affects the final structural complexity. In the studied Carboniferous turbidites the rheology of more thicken greywackes layers difficult homogeneous folding, leading to the development of conjugate shear zones during layer parallel shortening. In some cases, the thicker greywackes package indents the less competent shales from the external domains distorting the kink band boundaries. The structural anomalies induced by indentation of thick competent layers on kink boundaries, which is a strong evidence to the presence of fixed boundaries, have been described in others tectonic environments (*e.g.* Coke et al., 2003).

The rigid rotation of previous structures are unable to accommodate all the deformation inside the kink band. As there is no evidences of considerable volume loss and the orthogonal shortening must be balanced, either by sub-horizontal or sub-vertical stretching. The deformation induced by layer parallel shortening is heterogeneously distributed, being stronger in the vicinity of the kink band sub-vertical boundaries.

The internal dextral layer parallel slip induced the formation of monoclinic flexural folds, which also have an important role in the dissipation of the layer parallel shortening component. Indeed, such folds thickening the sequence orthogonally to the layering, in sub-horizontal plane. The relation of these folds to low plunging slickensides the presence of some vertical escape component, which appears to be non-negligible in the horizontal shortening dissipation.

In Abrantes N20ºE kink band, the structural pattern is simpler, with the development of a conjugate set of 2nd order kink bands during layer parallel shortening. These structures induce an orthogonal sub-horizontal thickening inside kink band. In these case, there are no evidences of layer parallel-slip within kink-band.

The trend of the sinistral 2nd order structures presents a counterclockwise rotation (usually less than 45º) in relation to the main kink band. The geometric and kinematic features

of these structures are similar to the "shear crenulations" (Matte, 1969; Stubley, 1990) or strain-slip crenulations, if slip along kink band boundaries was present (Matte, 1969). During the deformation, the angle between these 2nd order structures and the main kink band decrease (Matte, 1969), which could explain the trend dispersion of these structure. Such dispersion could also be enhanced by the presence of simple shear along the main sinistral kink band, as highlighted in experimental works (Williams and Price, 1990). The shear crenulations are pervasive in wider kink bands and could result from different mechanisms (Stubley, 1990) as reorientation of stress field due to rotation in relation to external layering or rotation of main kink band direction and the presence of shortening parallel to internal foliation. The presence of conjugate 2nd order kink bands allows to calculate the internal stress field that is compatible with layer parallel shortening within kink band, as previously mentioned.

The 2nd order sinistral kink bands are considered structures developed during widening of pre-existing kink bands (Stubley, 1990). However, in the Abrantes kink band the angular data seems to indicate type III fixed boundaries and, consequently, fixed width. Thus, the 2nd order structures seem to result from continuous deformation process in simple shear regime related to the main kink band with diffuse boundaries.

X.2.7. Final Remarks

The Almograve and Abrantes kink bands show strong similarities in their deformation mechanisms, although with particular features. This particularities allows the better understanding of the late stages of the Variscan Orogeny dynamics. The observed sinistral non-coaxial deformation of NNE-SSW kink bands and its brittle to brittle-ductile behaviour are compatible to previous models for this deformation episode (Ribeiro, 2002; Dias et al, 2016b).

In fixed hinge kink bands, the rotation of the internal domains related to its genesis induces the distortion of previous structures. This distortion could be easily estimated using the proposal graph based in the classical kink band angles. The strength of this new methodology was assessed by comparing the graphical estimations with values obtained by independent methods for two particularly well exposed kink band examples.

Nevertheless, care should be taken in the interpretation of the estimated shortening value, because slightly variations in the angular values could be induced, either by slip along kink band boundaries or by layer parallel slip.

The studied field examples show that during the development of type III fixed hinge kink bands, the strain is localized within kink band due the internal rotation of primary layering and/or slip along the kink boundaries. Thus, some internal structures should be developed due

to the distortion induced by the kink folding mechanism. These structures are mostly controlled by the rheology and heterogeneity of deformed sequence, coupled with layer parallel shortening and layer parallel slip mechanisms.

References

Anderson, T. B. (1964). Kink bands and related geological structures. Nature, 202, 272–274.

Anderson, T.B. (1974). The relationship between kink bands and shear fractures in the experimental deformation of slate. Journal of the Geological Society, 130, 367–382.

Arthaud, F., Matte, Ph. (1977). Late Paleozoic strike-slip faulting in southern Europe and northern Africa: result of a righ-lateral shear zone between the Appalachians and the Urals. Geological Society of America Bulletin, 88, 1305-1320.

Babaie, H.A., Speed, R.C. (1990). Origin of kink bands in the Golconda allochthon, Toiyabe Range, Nevada. Geological Society of America Bulletin, 102, 315-321.

Borg, I., Handin, J. (1966). Experimental deformation of crystalline rocks. Tectonophysics, 3, 249–368.

Carreras, J. (2001). Zooming on Northern Cap the Creus Shear Zones, Journal of Structural Geology, 23, 1457-1486.

Choukhroune, P., Iglésias, M. (1980). Zonas de cisalla dúctil en el NW de la Peninsula Ibérica. Cadernos Laboratorio Xeolóxico de Laxe, 1, 163-164.

Carreras, J., Julivert, M., Santanach, P. (1980). Hercynian Mylonite Belts in the Eastern Pyrenees: an example of shear zones associated with late folding. Journal of Structural Geology, 2, 5-9.

Caroça, C., Dias, R. (2002). Deformação transcorrente nos sectores externos da zona Sul Portuguesa; os últimos incrementos da tectónica Varisca. Comunicações do Instituto Geológico e Mineiro, 89, 115-126.

Cobbold, P.R., Cosgrove, J.W., Summers, J.M. (1971). Development of internal structures in deformed anisotropic rocks. Tectonophysics, 12, 23–53.

Coke, C., Dias, R., Ribeiro, A. (2003). Rheologically induced structural anomalies in transpressive regimes, Journal of Structural Geology, 25(3), 409-420.

Collomb, P., Donzeau, M. (1974). Relations entre kink bands decametriques et fractures de socle dans l'Hercynien des Monts d'Ougarta (Sahara Occidental, Algerie). Tectonophysics, 24 (3), 213–242.

Davies, R.K., Pollard, D.D. (1986). Relations between left-lateral strike-slip faults and right-lateral monoclinal kink bands in granodiorite, Mt. Abbot quadrangle, Sierra Nevada, California. Pure and Applied Geophysics, 124, 177–201.

Denèle, Y., Laumonier, B., Paquette, J., Olivier, Ph., Gleizes, G., Barbey, P. (2014). Timing of granite emplacement, crustal flow and gneiss dome formation in the Variscan segment of the Pyrenees. In: Schulmann, K., Martínez Catalán, J.R., Lardeaux, J.M., Janousek, V., Oggiano, G. (Eds.) The Variscan Orogeny: Extent, Timescale and the Formation of the European Crust. Geological Society of London, 405, 265-287.

Dewey, J.F. (1965). Nature and origin of kink bands. Tectonophysics, 1, 459–494.

Dewey, J. F. (1969). The origin and development of kink bands in a foliated body. Geological Journal, 6, 193-216.

Dias, R., Basile, C. (2013). Estrutura dos Sectores Externos da Zona Sul Portuguesa; Implicações Geodinâmicas. In: Dias, R., Araújo, A., Terrinha, P., Kullberg, J.C. (Eds.), Geologia de Portugal, vol. I, Escolar Editora, 787-805.

Dias, R., Ribeiro, A., Coke, C., Pereira, E., Rodrigues, J., Castro, P., Moreira, N., Rebelo, J. (2013). Evolução estrutural dos sectores setentrionais do autóctone da Zona Centro-Ibérica. In: Dias, R., Araújo, A., Terrinha, P., Kullberg, J.C. (Eds.), Geologia de Portugal, vol. 1, Escolar Editora, 73-147.

Dias, R., Moreira, N., Ribeiro, A. (2015). Dextral strike-slip tectonics in Iberia and the Pangeia Assemblage; evidences of the Tardi-Variscan Deformation event in South Portuguese Zone. The Variscan belt: correlations and plate dinamics. Géologie de la France (Variscan 2015 special issue, Rennes), 2015(1), 50-51.

Dias, R., Ribeiro, A., Romão, J., Coke, C., Moreira, N. (2016a). A review of the arcuate structures in the Iberian Variscides; constraints and genetical models. Tectonophysics, 681, 170-194. DOI:10.1016/j.tecto.2016.04.01

Dias, R., Moreira, N., Ribeiro, A., Basile, C. (2016b). Late Variscan Deformation in the Iberian Peninsula; A late feature in the Laurentia-Gondwana Dextral Collision. International Journal of Earth Sciences (Geol Rundsch). DOI: 10.1007/s00531-016-1409-x

Donath, F.A. (1961). Experimental study of shear failure in anisotropic rocks, Geological Society of America Bulletin, 72, 985-990.

Donath, F.A. (1968). Experimental study of kink bands in Martinsburg slate. In: Baer, A.J., Norris, D. K., (Eds.) Researches in tectonics. Geological Survey of Canada, 68-52, 255–288.

Dunham, R.E., Crider, J.G., Burmester, R.F., Schermer, E.R., Housen, B.A. (2011). Geometry, microstructures, and magnetic fabrics of kink bands in Darrington Phyllite, northwestern Washington, USA: processes within fixed-hinge kinking. Journal of Structural Geology, 33, 1627–1638.

Gay, N. C., Weiss, L. E. (1974). The relationship between principal stress directions and the geometry of kinks in foliated rocks, Tectonophysics, 21, 287-300.

Gleizes, G., Leblanc, D., Bouchez, J. (1997). Variscan granites of the Pyrenees revisited: their role as syntectonic markers of the orogen. Terra Nova, 9, 38–41.

Goscombe, B.D., Findlay, R.H., Mcclenaghan, M.P., Everard, J. (1994). Multiscale kinking in northeast Tasmania – crustal shortening at shallow crustal levels. Journal of Structural Geology, 16, 1077–1092.

Goswami, T.K. (2013). Kink band microstructures in Mica in the Dafla Formation of the Siwalik Group of rocks, West Kameng District, Arunachal Pradesh. International Journal of Scientific Research, 2 (12).

Hanmer, S.K. (1982). Vein arrays as kinematic indicators in kinked anisotropic materials. Journal of Structural Geology, 4(2), 151-160.

Hanmer, S., Corrigan, D., Ganas, A. (1996). Orientation of nucleating faults in anisotropic media: insights from three-dimensional deformation experiments. Tectonophysics, 267, 275-290.

Iglesias, M., Ribeiro, A. (1981). Zones de cisaillement ductile dans l'arc ibéro-armoricain. Comunicações dos Serviços Geológicos de Portugal, 67, 85-87.

Jensen, H.M. (1999). Analysis of compressive failure of layered materials by kink band broadening. International Journal of Solids and Structures, 36, 3427-3441.

Kirschner, D.L., Teixell, A. (1996). Three-dimensional geometry of kink bands in slates and its relationship with finite strain. Tectonophysics, 262, 195-211.

Lourenço, J., Mateus, A., Coke, C., Ribeiro, A. (2002). A zona de falha Penacova-Régua-Verín na região de Telões (Vila Pouca de Aguiar); alguns elementos determinantes da sua evolução em tempos tardivariscos. Comunicações do Instituto Geológio e Mineiro, 89, 105-122.

Marques, F., Mateus, A., Tassinari, C. (2002). The Late-Variscan fault network in central-northern Portugal (NW Iberia): a re-evaluation. Tectonophysics, 359, 255-270.

Marques, F., Burg, J., Lechmann, S., Schmalholz, S. (2010). Fluid-assisted particulate flow of turbidites at very low temperature: A key to tight folding in a submarine Variscan foreland basin of SW Europe. Tectonics, 29. DOI: 10.1029/2008TC002439

Mateus, A., Noronha, F. (2010). Sistemas mineralizantes epigenéticos na zona Centro-Ibérica;. In: Cotelo Neiva, J.M., Ribeiro, A., Mendes Victor, L., Noronha F., Magalhães Ramalho, M., (Eds.). Ciências Geológicas. Associação Portuguesa de Geólogos, 2, 47-62.

Matte, Ph. (1969). Les kink bands-example de deformation tardive dam l'Hercynien du nord-ouest de l'Espagne. Tectonophysics, 7, 309-322.

Martins, H., Sant'Ovaia, H., Noronha, F. (2009). Genesis and emplacement of felsic Variscan plutons within a deep crustal lineation, the Penacova-Régua-Verín fault: An integrated geophysics and geochemical study (NW Iberian Peninsula). Lithos, 111, 142–155.

Misra, S., Burg, J.P. (2012). Mechanics of kink bands during torsion deformation of muscovite aggregate. Tectonophysics, 548–549, 22–33.

Moreira, N. (2012). Caracterização estrutural da zona de cisalhamento Tomar-Badajoz-Córdova no sector de Abrantes. MSc thesis (unpublished), Évora University, Portugal, 225 p.

Moreira, N., Dias, R., Coke, C., Búrcio M. (2010). Partição da deformação Varisca nos sectores de Peso da Régua e Vila Nova de Foz Côa (Autóctone da Zona Centro Ibérica); Implicações Geodinâmicas. Comunicações Geológicas, 97, 147-162.

Moreira, N., Araújo, A., Pedro, J.C., Dias, R. (2014). Evolução geodinâmica da Zona de Ossa-Morena no contexto do SW Ibérico durante o Ciclo Varisco. Comunicações Geológicas, 101, 275-278.

Moreira, N., Pedro, J., Romão, J., Dias, R., Araújo, A., Ribeiro A. (2015). The Neoproterozoic-Cambrian transition in Abrantes Region (Central Portugal); Litostratigraphic correlation with Cambrian Series of Ossa-Morena Zone. The Variscan belt: correlations and plate dinamics. Géologie de la France, 2015(1), 101-102.

Moreira, N., Romão, J., Pedro, J., Dias, R., Ribeiro, A. (2016). The Porto-Tomar-Ferreira do Alentejo Shear Zone tectonostratigraphy in Tomar-Abrantes sector (Portugal). Geo-Temas, 16(1), 85-88. ISSN 1576-5172.

Nance, R.D., Gutiérrez-Alonso, G., Keppie, J.D., Linnemann, U., Murphy, J.B., Quesada, C., Strachan, R.A., Woodcock, N.H. (2012). A brief history of the Rheic Ocean. Geoscience Frontiers, 3, 125-135.

Pachell, M., Evans, J.P., Lansing Taylor, W. (2003). Kilometer-scale kinking of crystalline rocks in a transpressive convergent setting, Central Sierra Nevada, California. GSA Bulletin, 115 (7), 817–831.

Paterson, M.S., Weiss, L.E. (1962). Experimental folding in rocks. Nature, 195, 1046–1048.

Paterson, M.S., Weiss, L.E. (1966). Experimental deformation and folding in phyllite. Geological Society of America Bulletin, 77, 343–374.

Peacock, D.C.P. (1993). The displacement-distance method for contractional kink bands. Tectonophysics, 220, 13-21.

Peacock, D.C.P., Sanderson, D. J. (1995). Strike-slip relay ramps. Journal of Structural Geology, 17, 1351-1360.

Pereira, E., Ribeiro A., Meireles, C. (1993). Cisalhamentos hercínicos e controlo das mineralizações de Sn-W, Au e U na Zona Centro-Ibérica, em Portugal. Cadernos Laboratorio Xeolóxico de Laxe, 18, 89-119.

Pereira, M., Castro, A., Chichorro, M., Fernández, C., Díaz-Alvarado, J., Martí, M., Rodríguez, C., (2014). Chronological link between deep-seated processes in magma chambers and eruptions: Permo-Carboniferous magmatism in the core of Pangaea (Southern Pyrenees). Gondwana Research, 25, 290–308.

Qiao, L., Winey, K.I. (2000). Evolution of Kink Bands and Tilt Boundaries in Block Copolymers at Large Shear Strains. Macromolecules, 33, 851-856

Ramsay, J.G. (1962). The geometry of conjugate fold systems: Geological Magazine, 99, 516-526.

Ramsay, J.G. (1967). Folding and fracturing of rocks. McGraw-Hill, New York, 568 p.

Ramsay, J.G., Huber, M. (1987). The Techniques of Modern Structural Geology, Vol. 2: Folds and Fractures. Academic Press.

Ribeiro, A. (2002). Soft Plate Tectonics. Springer-Verlag, 324 p.

Ribeiro, A., Munhá, J., Dias, R., Mateus, A., Pereira, E., Ribeiro, L., Fonseca, P., Araújo, A., Oliveira, T., Romão, J., Chaminé, H., Coke, C., Pedro, J. (2007). Geodynamic evolution of the SW Europe Variscides. Tectonics, 26, TC6009, DOI:10.1029/2006TC002058.

Romão, J., Moreira, N., Dias, R., Pedro, J., Mateus, A., Ribeiro, A. (2014). Tectonoestratigrafia do Terreno Ibérico no sector Tomar-Sardoal-Ferreira do Zêzere e relações com o Terreno Finisterra. Comunicações Geológicas, 101(I), 559-562.

Sant'Ovaia, H., Noronha, F. (2005). Gravimetric anomaly modelling of the post-tectonic granite pluton of Águas Frias-Chaves (Northern Portugal). Cadernos Laboratorio Xeolóxico de Laxe, 30, 75-86.

Sant'Ovaia, H., Bouchez, J.L., Noronha, F., Leblanc, D., Vigneresse, J.L. (2000). Composite-laccolith emplacement of the post-tectonic Vila Pouca de Aguiar granite pluton (northern Portugal): a combined AMS and gravity study. Transactions of the Royal Society of Edinburgh: Earth Sciences, 91, 123-137.

Sharma, B.K., Bhola, A.M. (2005). Kink bands in the Chamba region, Western Himalaya, India. Journal of Asian Earth Sciences, 25, 513–528.

Sibson, R.H. (2012). Reverse fault rupturing: competition between non-optimal and optimal fault orientations. Geological Society London, Special Publications, 367, 39-50.

Srivastava, D. C., Lisle, R. J., Imran, M., Kandpal, R. (1998). The kink band triangle: a triangular plot for paleostress analysis from kink bands. Journal of Structural Geology, 20(11), 1579-1586.

Starkey, J. (1968). The Geometry of Kink Bands in Crystals - A Simple Model. Contributions to Mineralogy and Petrology, 19, 133-141.

Stewart, K.G., Alvarez, W. (1991). Mobile-hinge kinking in layered rocks and models. Journal of Structural Geology, 13(3), 243-259.

Stubley, M.P. (1990). The geometry and kinematics of a suite of conjugate kink bands, southeastern Australia. Journal of Structural Geology, 12, 1019–1031.

Suppe, J. (1985). Principles of Structural Geology. Prentice-Hall, New Jersey.

Suppe, J., Sábat, F., Muñoz, J.A., Poblet, J., Roca, E., Vergés, J. (1997). Bed-by-bed fold growth by kink band migration: Sant Llorenç de Morunys, eastern Pyrenees. Journal of Structural Geology, 9(3-4), 443-461.

Tchalenko, J. S. (1968). The evolution of kink bands and the development of compression textures in sheared clays. Tectonophysics, 6, 159-174.

Tobisch, O. T., Fiske, R. S. (1976). Significance of conjugate folds and crenulations in the central Sierra Nevada, California. Geological Society of America Bulletin, 87, 1411-1420.

Twiss, R. J., Moores, E. M. (1992). Structural Geology. W. H. Freeman and Company, New York.

Verbeek, E. R. (1978). Kink bands in the Somport slates, west central Pyrenees, France and Spain. Geological Society of America Bulletin, 89, 814-824.

Wadee, M. A. Edmunds, R. (2005). Kink band propagation in layered structures. Journal of the Mechanics and Physics of Solids, 53(9), 2017–2035.

Wadee, M. A., Hunt, G. W., Peletier, M. A. (2003). Kink band instability in layered structures. Journal of the Mechanics and Physics of Solids, 52(5), 1071–1091.

Weiss, L. E. (1968). Flexural slip folding of foliated model materials. Canadian Geological Survey Paper, 68-52, 294-359.

Weiss, L. E. (1980). Nucleation and growth of kink bands. Tectonophysics, 65, 1-38.

Williams, H.R. (1987). Stick-slip model for kink band formation in shear zones and faults. Tectonophysics, 140, 327-331.

Williams, P. F., Price, G. P. (1990). Origin of kink bands and shearband cleavage in shear zones: an experimental study. Journal of Structural Geology, 12, 145-164.